Atmos. Chem. Phys., 25, 959–977, 2025
https://doi.org/10.5194/acp-25-959-2025

Atmospheric Chemistry and Physics
Open Access
EGU

Seasonal investigation of ultrafine-particle organic composition in an eastern Amazonian rainforest

Adam E. Thomas[1], Hayley S. Glicker[1], Alex B. Guenther[2], Roger Seco[3], Oscar Vega Bustillos[4], Julio Tota[5], Rodrigo A. F. Souza[6], and James N. Smith[1]

[1]Department of Chemistry, University of California, Irvine, Irvine, CA, USA
[2]Department of Earth System Science, University of California, Irvine, Irvine, CA, USA
[3]Institute of Environmental Assessment and Water Research (IDAEA-CSIC), Barcelona, Catalonia, Spain
[4]Chemistry and Environment Center, Instituto de Pesquisas Energéticas e Nucleares, Cidade Universitária, São Paulo, Brazil
[5]Institute of Engineering and Geoscience, Universidade Federal do Oeste do Pará, Santarém, Brazil
[6]Escola Superior de Tecnologia, Universidade do Estado do Amazonas, Manaus, Brazil

Correspondence: James N. Smith (jimsmith@uci.edu)

Received: 17 July 2024 – Discussion started: 23 July 2024
Revised: 17 October 2024 – Accepted: 1 November 2024 – Published: 27 January 2025

Abstract. Reports on the composition of ultrafine particles (< 100 nm in diameter) in the Amazon are scarce, due in part to the fact that new-particle formation has rarely been observed near ground level. Ultrafine particles near the surface have nevertheless been observed, leaving open questions regarding the sources and chemistry of their formation and growth, particularly as these vary across seasons. Here, we present measurements of the composition of ultrafine particles collected in the Tapajós National Forest (2.857° S, 54.959° W) during three different seasonal periods: 10–30 September 2016 (SEP), 18 November–23 December 2016 (DEC), and 22 May–21 June 2017 (JUN). Size-selected (5–70 nm) particles were collected daily (for 22 h each day) using an offline sampler. Samples collected during the three time periods were compiled and analyzed using liquid chromatography coupled with Orbitrap high-resolution mass spectrometry. Our findings suggest a sustained influence of isoprene organosulfate chemistry on ultrafine particles from the different periods. We present chemical evidence that indicates that biological-spore fragmentation impacted ultrafine-particle composition during the late wet season (JUN), while chemical markers for biomass burning and secondary chemistry peaked during the dry season (SEP and DEC). Higher oxidation states and degrees of unsaturation were observed for organics in the dry season (SEP and DEC), suggesting greater extents of aerosol aging. Finally, applying a volatility parameterization to the observed compounds suggests that organic sulfur species are likely key drivers of new-particle growth in the region due to their low volatility compared to other species.

1 Introduction

Ultrafine aerosol particles (UAPs) (< 100 nm in diameter) are ubiquitous in the atmosphere, representing the largest fraction of ambient aerosol loading by number (Seinfeld and Pandis, 2006). Inhalation of these particles is linked to adverse health effects in many different parts of the human body as these particles are small enough to infiltrate deep into lung tissue, enter the bloodstream, and cross the blood–brain barrier (Calderón-Garcidueñas and Ayala, 2022; Li et al., 2021; Nassan et al., 2021; Allen et al., 2017). Ultrafine particles can form in the atmosphere from the condensation of low-volatility gases in a process known as new-particle formation (NPF), considered to be the dominant emission pathway for new particles in the atmosphere (Dunne et al., 2016). Though too small themselves to interact with sunlight at most wavelengths, newly formed particles serve as a significant source of larger particles that can scatter or absorb incident solar radiation, directly impacting the climate. In addition,

particles formed via NPF are estimated to account for up to 50 % of global cloud condensation nuclei (CCN), particles that can take up water and serve as seeds for cloud droplets (Gordon et al., 2017; Westervelt et al., 2013; Merikanto et al., 2009; Wang and Penner, 2009). Another study has suggested that UAPs themselves may directly impact cloud formation and drive precipitation over the Amazon Basin and other pristine areas by increasing the convective intensity of deep convective clouds (Fan et al., 2018), though this is still an area of active research (Varble et al., 2023). Critical to understanding UAP formation, as well as its impact on human health and climate, is information on the distribution and chemical composition of UAPs as observed in different environments.

Although it is known for its pristine air quality (Andreae et al., 2004), the Amazon Basin nevertheless serves as an aerosol source of global significance, thanks in part to its large area and abundant emissions of biogenic volatile organic compounds (BVOCs) (Guenther et al., 2012), directly impacting the global CCN budget and helping maintain stratospheric aerosol levels (Williamson et al., 2019; Weigel et al., 2011; Brock et al., 1995). The properties of aerosols formed exhibit seasonal variability, driven primarily by monthly differences in deposition (i.e., rainfall) and gas emissions (Alves et al., 2016). Despite this significance, the chemistry and dynamics of particle formation and growth over the Amazon are not completely understood. NPF is rarely observed near the ground (Martin et al., 2010), in contrast to findings from remote forested locations in other regions of the world, where NPF is observed more frequently (e.g., Andreae et al., 2022; Dada et al., 2018; Dal Maso et al., 2008). Nevertheless, periodic *bursts* of UAPs, where little to no growth is apparent, have been observed at ground level. For example, a multiyear statistical analysis of size distribution data collected at the Cuieiras forest reserve in central Amazonia revealed that nearly one-third of the days observed featured undefined bursts of UAPs that did not appear to grow from local ground-level NPF events (Varanda Rizzo et al., 2018). Although formation is rarely seen near the surface, studies have observed intense NPF activity in the Amazon free troposphere (Andreae et al., 2018; Fan et al., 2018; Wang et al., 2016), where gaseous precursors are thought to be brought by convective updrafts and nucleation occurs due to low temperatures and particle surface area conditions (Zhao et al., 2020; Williamson et al., 2019; Weigel et al., 2011). Freshly nucleated particles, in turn, can be brought to the boundary layer by convective downdrafts and can grow to larger sizes through coagulation and condensation of BVOC oxidation products (Andreae et al., 2018; Wang et al., 2016; Merikanto et al., 2009; Ekman et al., 2008). A recent study demonstrated that nucleation of organic vapors could serve as the primary formation pathway for these particles (Zhao et al., 2020), but the molecular identities of the species involved and their seasonal variability remain largely unknown. Direct observations of UAP composition could help elucidate these formation and growth pathways and bridge the gap between what is known about gas emissions and the composition of larger aerosol particles.

Secondary products of BVOCs seem to contribute substantially to aerosol particle mass in the Amazon Basin (Martin et al., 2010). Near the surface, UAP formation is thought to be primarily driven by the nucleation of sulfuric acid, due to its extremely low volatility, after which new-particle growth can occur through the reactive uptake and condensation of other low-volatility species, such as oxygenated organic molecules (Ehn et al., 2014; Sipilä et al., 2010). Isoprene, the dominant volatile organic compound (VOC) emitted by regional vegetation (Guenther et al., 2012), has been estimated to contribute substantially to aerosol particle mass principally via the condensation of products formed from reactions with OH radicals (Isaacman-VanWertz et al., 2016; Chen et al., 2015). One such product, an organosulfate formed from the heterogeneous uptake of isoprene epoxydiol (IEPOX) onto sulfuric acid seed particles, has been observed in central Amazonia across different seasons, accounting for up to $\sim 90\,\%$ of organic sulfate mass observed under low-NO_x conditions (Glasius et al., 2018). Secondary products of monoterpenes, such as 3-methyl-1,2,3-butanetricarboxylic acid (MBTCA) and pinic acid (Leppla et al., 2023; Kourtchev et al., 2016; Kubátová et al., 2000), have also been observed in particles from the Amazon, though perhaps at significantly lower mass concentrations compared to those of dominant isoprene markers, such as IEPOX organosulfate, as suggested by recent findings regarding PM_1 particles from central Amazonia (Glasius et al., 2018). Due to the lack of particle size resolution in these measurements, particularly in the ultrafine range, it is difficult to comment on the extent to which these species are relevant to particle formation or growth in the region. Glicker et al. (2019) indirectly observed IEPOX in UAPs in central Amazonia during the Observations and Modeling of the Green Ocean Amazon 2014–2015 (GoAmazon2014/5) experiment using a thermal-desorption chemical-ionization mass spectrometer. The dominant positive ion observed throughout the measurement period was tentatively identified as a product of IEPOX thermal decomposition (3-methylfuran (m/z 83)) (Allan et al., 2014), indicating the role that isoprene oxidation plays in new-particle growth in the region. Glicker et al. (2019) also observed significant changes in UAP composition between background (or pristine) periods and periods of anthropogenic emission influence from the city of Manaus (located 70 km west of the site). Distinct compositional differences between anthropogenic and background periods were also observed in larger particles (PM_1) using an aerosol mass spectrometer at the same site during a different time of the year (de Sá et al., 2019), highlighting the sensitivity of particle growth pathways to human activity in the Amazon. Besides urban emissions, biomass burning has been shown to have a significant impact on particle composition, particularly during months with less rainfall (e.g., de Sá

et al., 2019; Kourtchev et al., 2016). Encroaching influences from deforestation, wildfires, and drought are projected to increase in the coming decades (Flores et al., 2024), causing disturbances in the Amazon ecosystem and potentially intensifying regional climate change. There is already evidence showing that the distribution of BVOCs in the Amazon is in a state of transition in response to human activity (Yáñez-Serrano et al., 2020). Gaining molecular insights into the species responsible for regional particle formation is critical to efforts aimed at modeling how these processes could change – and thus impact – global climate systems in the future.

Here, we present tree-canopy-level observations of UAP molecular composition from a site located within the Tapajós National Forest in eastern Amazonia. To gain insight into the seasonal differences in the sources contributing to particle formation and growth in this region, UAPs were collected during September and December of 2016 (dry season) and June of 2017 (late wet season). With an annual rainfall of 1920 mm (Saleska et al., 2003), the Tapajós National Forest is comparatively drier than other extensive wet forests in Brazil and is, therefore, thought of as a predictive model forest for the larger Amazon ecosystem with respect to future climate change scenarios (Cox et al., 2000).

2 Methods

2.1 Site description

Measurements were performed at the BR-Sa1 Santarem-Km67-Primary Forest tower site, situated in the Tapajós National Forest (2.857° S, 54.959° W). The site is located ∼ 7 km west of kilometer 67 of the Santarém–Cuiabá highway and about 50 km south of Santarém, Pará, Brazil. This site is part of the AmeriFlux and Large-Scale Biosphere–Atmosphere Experiment in Amazonia (LBA) networks. The Tapajós National Forest primarily comprises old-growth evergreen species (Saleska, 2019) and experiences a wet season extending from January to June and a dry season from mid-July through December (da Rocha et al., 2009; Saleska et al., 2003).

2.2 Ultrafine-particle collection

Aerosol particles were sampled near the top of the tree canopy by connecting ground-level instruments to a 30 m long inlet constructed of 9.5 mm copper tubing, with sampling conducted at a flow rate of 13.5 L min^{-1} (Fig. S1 in the Supplement). UAPs (5–70 nm in mobility diameter) were impacted onto pre-baked aluminum foil substrates using a sequential spot sampler (Aerosol Devices Inc.) (Fernandez et al., 2014) after being size-selected with a nano-differential mobility analyzer (nano-DMA; Model 3085, TSI). Particles were introduced as samples into the analyzer at a flow rate of 3.2 L min^{-1}. It should be noted that particles with diameters greater than 100 nm could be sampled when using a nano-DMA for size selection, given what is known regarding the charge state distribution of aerosol particles after they pass through a polonium-210 neutralizer (Liu et al., 1986); however, this effect should be reduced when using a selected upper mobility diameter limit less than 100 nm, such as the 70 nm limit used here. Foil substrates were placed inside the wells of a 33-well rotating sample disk, which collected samples for a period of 22 h per well (from midnight to 22:00 LT each day), followed by a 2 h blank collection in a separate well (from 22:00 LT to midnight each day). The blank consisted of particle-free air, sampled by setting the voltage of the nano-DMA to zero, which efficiently removed all particles from the sample stream. Number size distributions of the collected particles were measured in parallel by counting selected UAPs using a mixing condensation particle counter (Model 1720, Brechtel Manufacturing Inc.). Periodic size distribution measurements from the "Km67" site, spanning the period from September 2016 to June 2017, are shown in Fig. S2. UAPs were collected for compositional analysis during three different seasonal periods – 10–30 September 2016, 18 November–23 December 2016, and 22 May–21 June 2017 – with the samples collected during these periods hereafter referred to as SEP, DEC, and JUN, respectively. After collection, the sample plates were wrapped in clean aluminum foil, sealed with Teflon tape, and stored at −4 °C for later analysis.

2.3 Liquid chromatography–mass spectrometry (LC-MS) analysis

Sample foils from each measurement period were pooled together into vials (1 month per vial) for extraction in 600 µL of acetonitrile (high-performance liquid chromatography (HPLC) grade, Sigma-Aldrich) for 5 h at room temperature (21 °C). Blank collection foils were pooled and extracted in the same manner and quantity to serve as background signals. Extracts were then transferred into clean vials and evaporated under a gentle stream of nitrogen to obtain a final volume of 50 µL.

An LC-MS methodology was adopted in the present study to ensure the acquisition of usable spectra with the very low sample volume available, as well as to reduce the artifact-inducing effects of ion suppression that have been observed in the analysis of complex organic aerosols with direct infusion (Kourtchev et al., 2020). Samples were analyzed using an ultrahigh-performance liquid chromatograph (Vanquish UHPLC, Thermo Fisher Scientific) coupled with an Orbitrap mass spectrometer (Q Exactive Plus, Thermo Fisher Scientific), which has a mass resolving power of $\sim 10^5$ at m/z 200 and is equipped with a heated-electrospray-ionization (HESI) inlet. A Luna Omega 1.6 µm Polar C18 column (150 × 2.1 mm; Phenomenex), heated to 30 °C, was used as the stationary phase, while an eluent system consisting of 0.1 % (v/v) formic acid in water (HPLC grade, Sigma Aldrich; eluent A) and 0.1 % formic acid in acetoni-

trile (HPLC grade, Sigma Aldrich; eluent B) was used as the mobile phase. A sample volume of 10 µL was injected at a flow rate of 300 µL min^{-1} and subjected to the following 22 min gradient elution: a 3.0 min hold using 95 % eluent A, an 11 min ramp to 95 % eluent B, a 2.0 min hold using 95 % eluent B, and a 6.0 min hold using 95 % eluent A. The HESI inlet was set to a potential of 2.5 kV and a capillary temperature of 320 °C, with inlet flows of 50, 10, and 1 units for sheath gases, auxiliary gases (heated to 300 °C), and sweep gases, respectively. Mass spectra with data-dependent tandem mass spectra (MS2) acquisition were used for the present study, where ions were scanned in the negative ion mode from 100–1500 amu (with an automatic gain control (AGC) target value of 10^6 and a maximum injection time (IT) of 100 ms), while the top three most abundant ions from each scan were selected with an isolation window of 0.4 m/z for MS2 analysis via higher-energy collisional dissociation (Olsen et al., 2007) (with an AGC target value of 5×10^4, a maximum IT of 100 ms, and normalized collision energy (NCE) levels stepped at 10 %, 30 %, and 50 %). Xcalibur software (version 3.1, Thermo Fisher Scientific) was used for data acquisition.

LC-MS data were processed following a methodology developed by Nizkorodov et al. (2011) that has previously been used in the analysis of organic aerosol samples (e.g., Baboomian et al., 2022; Maclean et al., 2021). Briefly, FreeStyle software (version 1.6, Thermo Fisher Scientific) was used to view and integrate ion chromatograms in the region where analyte signals were observed (1–10 min). Decon2LS software (Jaitly et al., 2009) was then used to extract peak positions and intensities. The peak signal from the blank extract sample was then subtracted from that of the sample extract. Due to uncertainty regarding whether the air sampled during the blank collections was representative of the air sampled during the particle collections, the background was treated as simply corresponding to whatever chemical contaminants were on the foil substrates themselves – that is, whatever peaks that should be in the blank extract at around the same level of intensity as that of the sample. Home-built LabVIEW programs (National Instruments Corp.) were used to remove peaks containing ^{13}C and ^{34}S isotopes and to assign analyte peaks with the following formula constraints: a $C_{1-40}H_{2-80}O_{1-35}N_{0-3}S_{0-2}$ composition, H/C ratios of 0.2–2.25, O/C ratios of 0–4, and double-bond equivalents (DBEs) of −0.5 to 16.5. Only peaks with m/z values ranging from 100 to 700 were considered for assignment due to the low analyte abundance above this range.

2.4 Volatility prediction

Compound volatility distributions were predicted using the assigned molecular formulae from high-resolution mass spectrometry (HRMS) data, following Li et al. (2016). Volatilities are reported in terms of the saturation concentration of the pure organic vapors (C_0), predicted using the following parameterization:

$$\log_{10}C_0 = (n_C^0 - n_C)b_C - n_O b_O - 2\frac{n_C n_O}{n_C + n_O}b_{CO} - n_N b_N - n_S b_S, \quad (1)$$

where n_C, n_O, n_N, and n_S refer to the number of carbon, oxygen, nitrogen, and sulfur atoms, respectively. Values used for the parametric coefficients n_C^0, b_C, b_O, b_N, and b_S were determined by following those provided for the CHO, CHON, and CHOS compound classes in Li et al. (2016).

2.5 Meteorology and complementary datasets

Back-trajectory frequency simulations lasting 6 h were calculated for the three seasonal periods discussed in this study using the NOAA Hybrid Single-Particle Lagrangian Integrated Trajectory (HYSPLIT) transport model (https://www.ready.noaa.gov/HYSPLIT.php, last access: 15 March 2024) with a Global Data Assimilation System (GDAS) 1° meteorology (Rolph et al., 2017; Stein et al., 2015). Fire occurrence data were visualized using the Fire Information for Resource Management System (FIRMS) from NASA (https://www.earthdata.nasa.gov/learn/find-data/near-real-time/firms, last access: 20 May 2024), which compiles thermal-anomaly data obtained from the Moderate Resolution Imaging Spectroradiometer (MODIS) instruments aboard the Terra and Aqua satellites (data disclaimer link: https://www.earthdata.nasa.gov/learn/find-data/near-real-time/citation#ed-lance-disclaimer, last access: 20 May 2024) (Giglio et al., 2018). Meteorological ERA5 reanalysis data from the European Centre for Medium-Range Weather Forecasts (Hersbach et al., 2023) were obtained from the Climate Data Store (https://cds.climate.copernicus.eu, last access: 12 June 2024) to acquire parameters such as surface temperature, dew point temperature, precipitation, solar radiation at the surface, cloud cover, total atmospheric column water, boundary layer height, cloud base height, and leaf area index for the measurement site (2.9° S, −55° W), with a 0.25° resolution applied during each collection period.

3 Results and discussion

Figure 1 shows the average mass spectra obtained for the JUN, SEP, and DEC samples. Only assigned species are shown, corresponding to 77 %, 92 %, and 76 % of the total ion intensity attributed to the JUN, SEP, and DEC samples, respectively. The ion peaks are color-coded based on their assigned molecular formulae, categorized into four compound classes: CHO (green), CHON (blue), CHOS (red), and CHONS (purple). Also included are the ion-intensity-based distributions of each compound class across the different months. The percentage values shown correspond to the fraction of the total assigned ion intensity attributed to

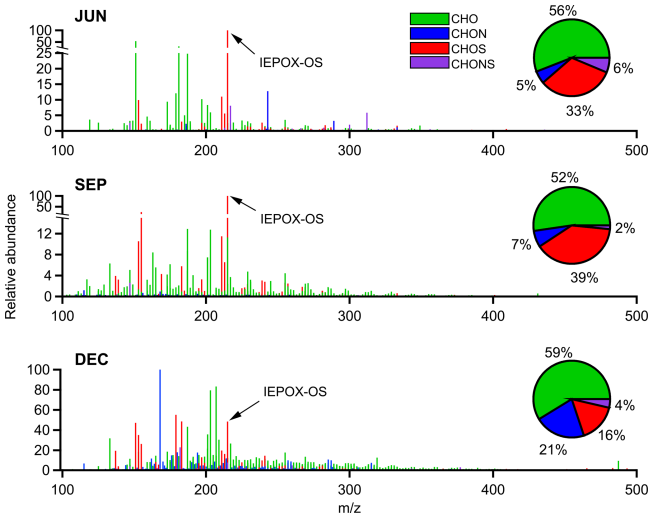

Figure 1. Average mass spectra of assigned species for the 3 months sampled. The colors of the individual peaks indicate the assigned compound classes: CHO (green), CHON (blue), CHOS (red), and CHONS (purple). On the right side of each spectrum, an overlaid pie chart displays the summed ion abundance of each compound class as a fraction of the total assigned intensity.

the sum of the species from each of the four compound classes. The CHO class (i.e., species only containing carbon, hydrogen, and oxygen atoms) accounted for the majority of the assigned intensity over all 3 months (52 %–59 %). The CHOS class was the second-most abundant category in JUN and SEP, while the CHON class was more dominant in DEC. CHONS compounds represented the smallest class observed, accounting for only 2 %–6 % of the assigned ion intensity. The single most abundant ion identified in both JUN and SEP had an m/z value of 215.0231, corresponding to a compound with the electrically neutral molecular formula $C_5H_{12}O_7S$. The molecule is tentatively identified as an IEPOX-derived organosulfate (IEPOX-OS) species based on its formula and the prominent loss of bisulfate (HSO_4^-) in its MS2 fragmentation spectrum (Fig. S3), a distinguishing feature of organosulfate species (Attygalle et al., 2001). It is noted that the relative peak intensity of this and other organosulfate species detected could be misleading when compared with that of other organic ions present as electrospray ionization (ESI) is known to be particularly sensitive to organosulfate compounds (Surratt et al., 2008). As noted above, IEPOX-OS species have been observed previously in Amazon aerosol particles (Glasius et al., 2018; Kourtchev et al., 2016), and their persistent presence in the ultrafine particles observed here, irrespective of season, implicates isoprene organosulfate chemistry as a key player in new-particle growth in the Amazon year-round. Despite this consistency, the UAPs sampled also exhibited substantial compositional variation, offering evidence of seasonal variability in emission sources and formation pathways.

3.1 Seasonality of marker ion distributions

Summaries of different species that are representative of key sources and processes, herein referred to as marker ions, have been provided for each month and are shown in Fig. 2a. The species listed represent five different potential sources based on their assigned molecular formulae: primary biogenic organic aerosol (PBOA), sesquiterpene-derived secondary organic aerosol (SQT SOA), monoterpene-derived secondary organic aerosol (MT SOA), isoprene-derived secondary organic aerosol (isoprene SOA), and biomass-burning organic aerosol (BBOA). Together, the included marker species account for 56 %, 42 %, and 17 % of the total assigned ion intensity (or 43 %, 38 %, and 13 % when including the unassigned intensity) for JUN, SEP, and DEC, respectively. Table S1 shows a full list of the markers identified, along with suggested chemical structures and references. It should be noted that since ion percentages are calculated as averages over analyte retention times (and since most identifications are based solely on the molecular formulae assigned), the ion signal attributed to species with these formulae may include several isomers. Although CHO compounds accounted for the largest fraction of ion intensity across all 3 months sampled, the most abundant species contributing to this compound class varied with the season. During the late wet season (JUN), the two most abundant CHO compounds had m/z values of 151.0612 (corresponding to the electrically neutral formula $C_5H_{12}O_5$) and 181.0718 ($C_6H_{14}O_6$) and were tentatively identified as the sugar alcohols arabitol and mannitol, respectively. These two species have previously been used as markers for PBOA (Samaké et al., 2019; Nirmalkar et al., 2015; Bauer et al., 2008) and are found in fungal spores, where they are used as energy storage products (Lewis and Smith, 1967). Lawler et al. (2020) previously observed these species in UAPs in the southeastern US using thermal-desorption chemical-ionization mass spectrometry and found that the concentration of UAPs containing these species spiked during periods of heightened rainfall. The study concluded that the observed UAPs formed from fungal spores, which fragmented upon exposure to rainfall and/or high humidity. Biological-spore samples collected in the Amazon have previously been observed to fragment under high-humidity conditions, such as those commonly observed during the wet season, resulting in the formation of UAPs (China et al., 2016). High concentrations of airborne fungal spores have also been linked to rainfall events (Huffman et al., 2013), and particles enriched in biogenic salts linked to fungal spores have been observed during the Amazon wet season (Pöhlker et al., 2012; Lawson and Winchester, 1979). To the best of our knowledge, our observations here represent the first chemical evidence of the occurrence of airborne ultrafine fungal fragments in the Amazon rainforest, presenting a previously unaccounted source of UAPs in the region. The fact that these ions were most abundant in JUN suggests that this process may be particularly important

(a)

	m/z	Molecular Formula	% Ion Abundance JUN	SEP	DEC
PBOA	151.0612	$C_5H_{12}O_5$	7.520	0.048	N.D.
	179.0561	$C_6H_{12}O_6$	1.696	N.D.	N.D.
	181.0718	$C_6H_{14}O_6$	4.445	N.D.	N.D.
SQT SOA	237.1496	$C_{14}H_{22}O_3$	N.D.	0.003	N.D.
	255.1238	$C_{13}H_{20}O_5$	0.497	0.654	0.359
	265.1440	$C_{15}H_{22}O_4$	0.033	0.011	0.043
	267.1232	$C_{14}H_{20}O_5$	0.109	0.156	0.125
	267.1596	$C_{15}H_{24}O_4$	0.035	N.D.	0.062
	269.1389	$C_{14}H_{22}O_5$	0.256	0.361	0.274
	271.1545	$C_{14}H_{24}O_5$	0.076	0.107	0.149
	285.1344	$C_{14}H_{22}O_6$	N.D.	0.232	0.150
	285.1702	$C_{15}H_{26}O_5$	0.053	0.069	0.117
	301.1293	$C_{14}H_{22}O_7$	0.101	N.D.	N.D.
MT SOA	147.0299	$C_5H_8O_5$	0.450	0.749	0.234
	173.0455	$C_7H_{10}O_5$	1.315	N.D.	0.376
	173.0819	$C_8H_{14}O_4$	N.D.	0.291	N.D.
	175.0612	$C_7H_{12}O_5$	0.281	0.241	0.169
	187.0612	$C_8H_{12}O_5$	3.481	1.906	0.880
	203.0561	$C_8H_{12}O_6$	0.836	1.886	0.258
	215.0561	$C_9H_{12}O_6$	0.789	1.667	0.188
	231.0510	$C_9H_{12}O_7$	0.203	0.474	0.106
	233.0667	$C_9H_{14}O_7$	0.047	0.205	0.034
	247.0823	$C_{10}H_{16}O_7$	0.055	0.146	0.050
Isoprene SOA CHO/CHON	119.0350	$C_4H_8O_4$	0.511	0.292	N.D.
	133.0142	$C_4H_6O_5$	N.D.	0.933	0.646
	135.0663	$C_5H_{12}O_4$	0.096	0.018	0.011
	144.0302	$C_5H_7O_4N$	0.038	0.043	0.033
	149.0456	$C_5H_{10}O_5$	0.465	N.D.	N.D.
	163.0248	$C_5H_8O_6$	0.073	1.243	0.093
	221.0667	$C_8H_{14}O_7$	0.099	0.086	N.D.
	235.1187	$C_{10}H_{20}O_6$	0.043	N.D.	0.004
	253.1293	$C_{10}H_{22}O_7$	0.103	0.012	N.D.
Isoprene SOA CHOS	138.9707	$C_2H_4O_5S$	0.007	0.475	0.083
	152.9863	$C_3H_6O_5S$	1.393	1.560	0.714
	154.9656	$C_2H_4O_6S$	0.324	3.707	0.535
	168.9812	$C_3H_6O_6S$	0.099	0.635	N.D.
	182.9969	$C_4H_6O_6S$	0.417	0.852	0.987
	184.9761	$C_3H_6O_7S$	N.D.	0.164	0.034
	197.0125	$C_5H_{10}O_6S$	0.358	0.483	0.265
	198.9918	$C_4H_6O_7S$	0.194	N.D.	0.151
	210.9918	$C_5H_6O_7S$	1.544	1.696	0.400
	213.0074	$C_5H_{10}O_7S$	0.785	0.967	0.332
	215.0231	$C_5H_{12}O_7S$	14.040	14.784	0.986
	229.0024	$C_5H_{10}O_8S$	0.198	0.350	0.042
	231.0180	$C_5H_{12}O_8S$	0.184	0.155	0.012
	315.0755	$C_{10}H_{20}O_9S$	0.047	0.010	0.012
BBOA	168.0302	$C_7H_7O_4N$	N.D.	0.139	2.034
	207.0510	$C_7H_{12}O_7$	0.126	0.246	1.693
	209.0457	$C_{10}H_{10}O_5$	N.D.	0.207	0.618

(b)

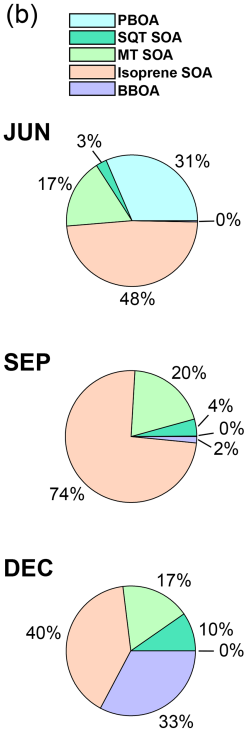

Figure 2. Distribution of emission marker species observed during each month. **(a)** Heatmap of individual ion abundances normalized by the total ion abundance (assigned and unassigned), expressed as percentages. The colors correspond to different emission source classes: primary biogenic organic aerosol (PBOA; blue), sesquiterpene-derived secondary organic aerosol (SQT SOA; dark green), monoterpene-derived secondary organic aerosol (MT SOA; light green), isoprene-derived secondary organic aerosol (isoprene SOA; yellow and orange), and biomass-burning organic aerosol (BBOA; purple). For each ion, darker shades correspond to a greater normalized abundance of that species relative to other months. "N.D." indicates that the species was not detected. **(b)** Pie charts showing the contribution of each emission source class as a percentage of the total marker ion intensity.

during the wet season, but more measurements are needed to confirm its spatiotemporal prevalence. In addition to arabitol and mannitol, another abundant CHO species in JUN was glucose ($C_6H_{12}O_6$ (m/z 179.0561)), a known marker of plant material such as pollen fragments (Samaké et al., 2019).

The most abundant CHO species in SEP were likely derived from monoterpene oxidation. To help corroborate this, the ion chromatograms and tandem mass spectra obtained for some of these species were compared to those of species observed in α-pinene ozonolysis particles. Bulk ozonolysis particles were collected in a series of laboratory experiments using the spot sampler, operating under conditions similar to those used in the present study. Details of these experiments are provided in the Supplement. The most abundant species observed was $C_8H_{12}O_5$ (m/z 187.0607), identified as one or more isomers of hydroxyterpenylic acid, a proposed marker for α-pinene oxidation (Kahnt et al., 2014). Similar fragments are observed when comparing the MS2 spectrum for this ion to the literature, including the dominant product ion ($C_6H_5O_3^-$) at m/z 125.0239 (Fig. S4). This species was also the most abundant monoterpene oxidation marker identified in JUN and DEC, suggesting that this compound may serve as a suitable marker at different times of the year in the Amazon. An unknown species (excluded from Fig. 2a) with the same unit mass (m/z 187.0976 ($C_9H_{16}O_4$)), found in both SEP and DEC, has a retention time similar to that of an α-pinene ozonolysis product observed in our experiments (Fig. S5), although it is likely that several isomers are present with different retention times. The second-most abundant CHO species in SEP had the molecular formula $C_8H_{12}O_6$ and was identified as 3-methyl-1,2,3-butanetricarboxylic acid (MBTCA), a marker for the multigenerational oxidation of monoterpenes (Szmigielski et al., 2007). Other studies have found MBTCA in particles from the central Amazon, with higher signals observed in the dry season (Glasius et al., 2018; Kourtchev et al., 2016) compared to the wet season. This is consistent with the idea that photochemical processing may be more prominent during the dry season, when more solar radiation is likely to penetrate the surface, reaching a maximum around August–September in the nearby city of Santarém (Reis et al., 2022). Corroborating this, ERA5 reanalysis data from the measurement site also show that the highest average daytime solar radiation at the surface occurred in SEP (Table S2). It is also worth noting that monoterpene emissions have been observed to peak during the Amazon dry season (Alves et al., 2022; Yáñez-Serrano et al., 2018), which helps explain the overall abundance of these markers in SEP. Comparison of the MS2 spectrum for this ion with that of a product with a similar retention time from the α-pinene ozonolysis experiments suggests structural similarities, including evidence of more than one carboxylic acid group (Figs. S6 and S7). It is intriguing that the lower-molecular-weight MT SOA markers generally have their highest abundance in JUN, whereas the heavier species, starting with $C_8H_{12}O_6$, have their highest abundance in SEP, possibly suggesting a seasonal dependence of reaction branching ratios. Another possible driver of these differences is the seasonal dependence of monoterpene speciation. For instance, Yáñez-Serrano et al. (2018) observed stark seasonal differences in monoterpene distributions in central Amazonia, noting a higher relative abundance of α-pinene and limonene during the dry season (August and October) and of α-terpinene and 3-carene in the late wet season (June). The species $C_5H_8O_5$, identified as 3-hydroxyglutaric acid

(Claeys et al., 2007), has also been observed as an oxidation product of isoprene from a non-IEPOX pathway (J. Liu et al., 2016; Krechmer et al., 2015), although it is used as a monoterpene marker here since the IEPOX pathway is likely to dominate during the Amazon wet season (Shrivastava et al., 2019). Relative to JUN and SEP, DEC had a lower contribution of secondary markers from both monoterpenes and isoprene. It should be noted that other compounds of anthropogenic origin, such as aromatic hydrocarbons, may also drive unaccounted secondary formation. Previous oxidation flow reactor measurements of ambient gases conducted in the central Amazon showed that a large fraction of observed SOA formation during the dry season could not be reconciled using the known formation potentials of terpenoids alone (Hodshire et al., 2018; Palm et al., 2018). In addition to monoterpene markers, several sesquiterpene oxidation products were also observed (Fig. 2a), albeit in a comparatively lower abundance. The most abundant product identified had the molecular formula $C_{13}H_{20}O_5$ (m/z 255.1238), with a suggested identity of β-nocaryophyllonic acid, a multigenerational oxidation product of β-caryophyllene previously identified in central Amazon PM_1 particles (Yee et al., 2018). In general, observed sesquiterpene products were most abundant in SEP, accounting for 1.6 % of the total ion intensity (assigned and unassigned) compared to 1.2 % in DEC and JUN, consistent with the occurrence of peak abundance in observed monoterpene products. It is notable, however, that these ion fractions are the most consistent between the three samples compared to all the other emission source classes, suggesting that sesquiterpene chemistry may serve as a year-round source of ultrafine-particle growth in the region.

In all 3 months, isoprene SOA accounted for the largest fraction of the identified marker ion intensity (Fig. 2b). Isoprene organosulfates were the most dominant isoprene-derived compounds observed each month and accounted for the highest ion abundance in SEP (28 % of the assigned intensity). Isoprene emissions and the formation of gas-phase oxidation products, such as IEPOX, typically peak in the Amazon dry season due to higher solar intensity and ambient temperatures relative to the wet season (Langford et al., 2022; Rinne et al., 2002), conditions reflected here in a comparison between JUN and SEP (Table S2). Sarkar et al. (2020) observed a strong correlation between the fluxes of isoprene and monoterpene and both temperature and solar radiation at the same measurement site in the Tapajós National Forest. Riva et al. (2019) found that increasing the concentration ratio of IEPOX to inorganic sulfate drives the formation of organosulfate species. The dominance of these species in SEP suggests that this ratio could be a key driver of organosulfate chemistry in the eastern Amazon and parallels observations of PM_1 composition from the central Amazon, where organic sulfate concentrations peaked in the dry months (Glasius et al., 2018). However, seasonal measurements of inorganic sulfate concentrations in UAPs are needed to further probe the influence of this chemistry. Compared to the other months, SEP also had the lowest average relative humidity (Table S2). Several studies have correlated organosulfate formation with aerosol acidity and observed an increased uptake of isoprene products, such as IEPOX, onto acidic particles (Zhang et al., 2018; Liao et al., 2015; Surratt et al., 2007b). Another possible explanation for the dominance of organosulfates in SEP could, therefore, be that less water vapor was available to dilute the sulfate aerosols needed to form these species, allowing for more efficient reactive uptake.

Though comprising the largest source fraction, the relative contribution of isoprene organosulfates to sample intensity was nevertheless at its smallest in DEC, most notably with regard to IEPOX-OS. Corresponding to the end of the dry season and the onset of the wet season, one possible explanation for this pertains to meteorology, given that DEC had the highest average cloud cover (82 %) and greatest amount of total column water (52 kg m^{-2}) of the 3 months studied (Table S2), possibly leading to reduced IEPOX formation and uptake for the reasons discussed above. Another possible factor could be the higher regional levels of NO_x due to wildfire activity, leading to the suppression of the IEPOX pathway via NO (Paulot et al., 2009). Although isoprene is generally expected to eventually form IEPOX via the HO_2 oxidant pathway under pristine conditions, Y. Liu et al. (2016) provided evidence that under polluted conditions, where $[NO_y] > 1$ ppb, isoprene photooxidation chemistry drastically shifts toward the NO pathway, producing oxidation products, such as methyl vinyl ketone, instead of HO_2-produced hydroxyhydroperoxide (ISOPOOH). At the same measurement site in the central Amazon (located 70 km west of the urban center of Manaus), Liu et al. (2018) found that OH concentrations, inferred from measured concentrations of isoprene photooxidation products, increased by 250 % under similar polluted conditions, indicating that the anthropogenic contribution of NO_x has the potential to greatly impact oxidation pathways. Figure 3a shows an air mass history analysis using HYSPLIT, and Fig. 3b shows the distribution of fires observed by the MODIS instruments via satellite during each of the three seasonal periods. Although each period was dominated by easterly winds, the number of fires observed varied substantially, with most anomalies occurring in DEC. Corroborating the satellite data is the abundance of identified BBOA species observed in DEC, including $C_7H_7O_4N$, $C_7H_{12}O_7$, and $C_{10}H_{10}O_5$, assigned to methyl-nitrocatechol, methyl galacturonate, and a vanillin oxidation marker, respectively (Go et al., 2022; Kong et al., 2021; Iinuma et al., 2010). Under the influence of NO_x, isoprene reacts with OH radicals and NO/NO_2 to form methacryloyl peroxynitrate, which then can be oxidized to form the aerosol markers 2-methylglyceric acid and 2-methylglyceric acid organosulfate (2-MG-OS) (Nguyen et al., 2015; Surratt et al., 2007b). Compared to IEPOX-OS, 2-MG-OS ($C_4H_8O_7S$ (m/z 198.9918)) was observed to be a comparatively minor species, but it is notable that the ratio of

2-MG-OS to IEPOX-OS was an order of magnitude higher in DEC than in JUN (Fig. 2a), the month experiencing the least influence from regional wildfire activity (Fig. 3b). The only organosulfate species that had a greater relative contribution to ion intensity in DEC than in the other months was $C_4H_8O_6S$ (m/z 182.9969). Shalamzari et al. (2013) observed this compound in ambient filters from Hungary and, through structural characterization via multistage mass spectrometry (MSn) analysis, hypothesized that the species was formed from the oxidation of methyl vinyl ketone, a first-generation isoprene product formed via ozonolysis or by OH oxidation in the presence of NO_x (Liu et al., 2013; Barket et al., 2004; Aschmann and Atkinson, 1994). Besides isoprene oxidation, methyl vinyl ketone can also be emitted from the biomass burning of tropical forest fuels (Karl et al., 2007). Additionally, two nitrooxy isoprene organosulfate (OS) species (Surratt et al., 2008) were identified in the dry-season months (SEP and DEC) (Table S1 in the Supplement): $C_5H_{11}O_9NS$ and $C_5H_9O_{12}N_2S$. The identification of these species further supports the hypothesis that isoprene chemistry may have been influenced by NO_x enrichment in the dry season. In addition to wildfire activity, it is also likely that traffic emissions from the Santarém–Cuiabá highway, located $\sim$7 km east of the measurement site, contribute to local NO_x concentrations. Given the dominance of easterly winds during sampling in each period (Fig. 3a), local highway emissions could potentially impact particle chemistry near the site and throughout the larger Tapajós National Forest area year-round, and they may serve as a particularly important source of NO_x in the forest during the wet season, when fire activity is low. Besides the influence from NO_x emissions, it should be noted that biomass burning can also serve as a source of SO_2 and sulfate (Rickly et al., 2022; Ren et al., 2021). Overall, these observations suggest that anthropogenic emission sources, such as biomass burning, may impact isoprene organosulfate formation processes in Amazonian UAPs – impacts likely to increase in coming decades with further human activity in the region.

Organic sulfur compounds from sources other than isoprene were also identified in all three samples, but they were most prominently represented in SEP and DEC (Table S1). For instance, the most abundant CHOS species in DEC was $C_6H_{12}O_4S$ (m/z 179.0385), which is attributed to the SO_2-initiated photooxidation of polycyclic aromatic hydrocarbons, such as those emitted during biomass burning (Jenkins et al., 1996), and dimethyl sulfoxide (DMSO) (Jiang et al., 2022), an oxidation product of dimethyl sulfide (DMS), a compound associated with marine emissions (Andreae and Raemdonck, 1983) and biomass burning (Meinardi et al., 2003). Other abundant CHOS species in DEC, possibly derived from similar sources, include $C_4H_8O_4S$ and $C_2H_4O_6S$ (Jiang et al., 2021; Kuang et al., 2016). Monoterpene-derived organosulfate (MT-OS) species were also identified, though in low abundance relative to isoprene-derived organosulfates, with the sum of MT-OS compounds for each month contributing less than 0.7 % to the total ion signal. Interestingly, when comparing the different months, DEC exhibited the highest number of MT-OS compounds (eight in total), including $C_7H_{12}O_7S$, $C_9H_{16}O_6S$, and $C_7H_{12}O_6S$. In addition, two nitrooxy MT-OS species were identified and were solely present in DEC: $C_{10}H_{17}O_7NS$ and $C_9H_{15}O_8NS$. These species have previously been proposed to form from either nitrate radical oxidation or photooxidation in the presence of NO_x, both occurring in the presence of acidic sulfate particles (Surratt et al., 2008).

Species with molecular formulae pertaining to non-organosulfate isoprene markers were also identified in each month (Fig. 2A); these included 2-methyltetrol ($C_4H_8O_4$ (m/z 119.0350)) and 2-methyltartaric acid ($C_5H_8O_6$ (m/z 163.0250)) (Jaoui et al., 2019; Claeys et al., 2004). Interestingly, most of the CHO isoprene markers identified were most abundant in JUN. Given that this month experienced the highest average relative humidity, a possible explanation is that these products were formed under less acidic conditions in particles, hindering subsequent oxidation by sulfuric acid and the formation of their organosulfate counterparts. Regarding possible humidity effects, it is also worth noting that 2-methyltetrol, formed via the particle-phase hydrolysis of IEPOX, and its dimer ($C_{10}H_{22}O_7$ (m/z 253.1293)) are most abundant in JUN (Armstrong et al., 2022; Riva et al., 2019; Surratt et al., 2007a). Conversely, the IEPOX-OS dehydration product $C_5H_{10}O_6S$ (m/z 197.0125) is most abundant in SEP, the driest month observed. Finally, a marker for the oxidation of isoprene by the nitrate radical was also identified ($C_5H_7O_4N$ (m/z 144.0302)) (Rollins et al., 2009). The ion fraction of this species was relatively consistent across all 3 months, suggesting that this process may serve as a regular source of UAP growth in the region (likely occurring during the nighttime due to reactions with nitrate), irrespective of the season.

3.2 Seasonality of aerosol molecular properties

In addition to differences in the marker ions, differences in the molecular properties of all species observed in each month, such as the distribution of oxidation states and degrees of unsaturation, were also investigated. Figure 4 depicts the carbon oxidation states and double-bond equivalents of the CHO-containing molecules observed during each period. The carbon oxidation state (OS_C) was estimated following Kroll et al. (2011):

$$OS_C \approx 2O/C - H/C, \quad (2)$$

where O/C and H/C refer to the ratio of oxygen to carbon atoms and the ratio of hydrogen to carbon atoms, respectively. It should be noted that the presence of certain functionalities, such as peroxides, will lead to an overestimation of the carbon oxidation state. Nevertheless, this estimate serves as a relative means of comparing the extent of oxidation of the molecules from each period. Most species

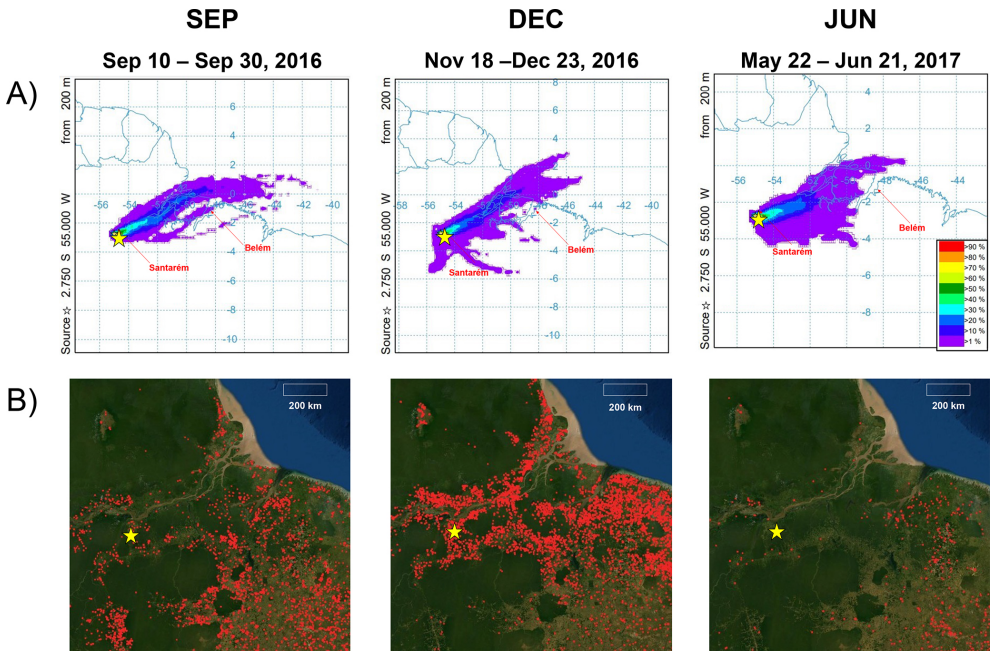

Figure 3. **(a)** Air mass back-trajectory frequencies from the HYSPLIT model for each seasonal period studied; 48 h back trajectories were integrated over the time span of each period at a height of 200 m above ground level (near the tree canopy). The color scale indicates how frequently air masses passed over a given location, with warmer colors indicating higher frequencies. **(b)** MODIS fire observations from the Aqua and Terra satellites, as visualized using FIRMS, integrated over each period. Each red dot indicates a thermal anomaly identified as a probable fire occurrence. The yellow star in each plot indicates the location of the measurement site.

observed had OS_C values between −1 and 1, corresponding to the oxidation range associated with semivolatile and low-volatility oxidized organic aerosol components (Kroll et al., 2011). Compared to JUN, higher oxidation states were observed in SEP and DEC across most carbon numbers. Using measurements of reactive gases, previous studies have shown that OH reactivity is highest during the Amazon dry season (Pfannerstill et al., 2021; Nölscher et al., 2016), coinciding with the seasonal peak in BVOC emissions and sunlight. These factors, coupled with the fact that potentially fewer products are lost due to wet deposition, can thus be thought of as optimized for the multigenerational oxidation of organics during the dry season. Higher-molecular-weight CHO species were also observed in SEP and DEC. Baboomian et al. (2022) found that UV-aged SOA components were, on average, more oxidized, more unsaturated, and heavier than those from fresh aerosol, attributing this to condensed-phase photochemical reactions. In line with this, CHO species observed in JUN were also more saturated compared to those observed in SEP and DEC (Fig. 4b). Besides the possible influence of photochemistry, biomass-burning organics can also be highly unsaturated, with oxygenated aromatic and nitroaromatic species serving as known markers (Bianchi et al., 2019; Iinuma et al., 2010).

Figure 5 depicts the distribution of highly unsaturated CHON molecules (with six or more DBEs) across the periods. CHON was the smallest compound class in JUN in terms of ion abundance and had the lowest number of observed molecular formulae (65 molecules assigned), most of which were relatively saturated. While more unsaturated species were observed in SEP, the most highly unsaturated CHON species were observed in DEC, possibly due to the influence of wildfires. Kourtchev et al. (2016) observed a similar trend in bulk organic aerosol collected from central Amazonia, also suggesting the influence of BBOA aromatics. Figure S8 shows a similar trend for CHO molecules. Figure 6 depicts the distribution of CHON species in van Krevelen space. In addition to being more saturated, CHON molecules observed in JUN were also less oxidized compared to those observed in the peak dry season (SEP), suggesting that aging processes (such as photochemistry), which may affect the CHO fraction, likely also influence nitrogen-containing species in the dry months. A similar trend is observed when comparing JUN to DEC (Fig. S9), though most of the most abundant ions appear to have similar O/C ratios.

Using a molecular corridor parameterization (Li et al., 2016), the volatilities of UAP constituents were estimated for each compound class (Fig. 7) to investigate relative changes in the species volatility distributions across the different seasons. Most species observed in each period were classified as either semivolatile organic compounds (SVOCs), defined as having a saturation mass concentration (C_0) between 0.3 and 300 $\mu g\,m^{-3}$, or low-volatility organic compounds (LVOCs) ($3 \times 10^{-4} < C_0 < 0.3\,\mu g\,m^{-3}$) (Murphy et al., 2014; Don-

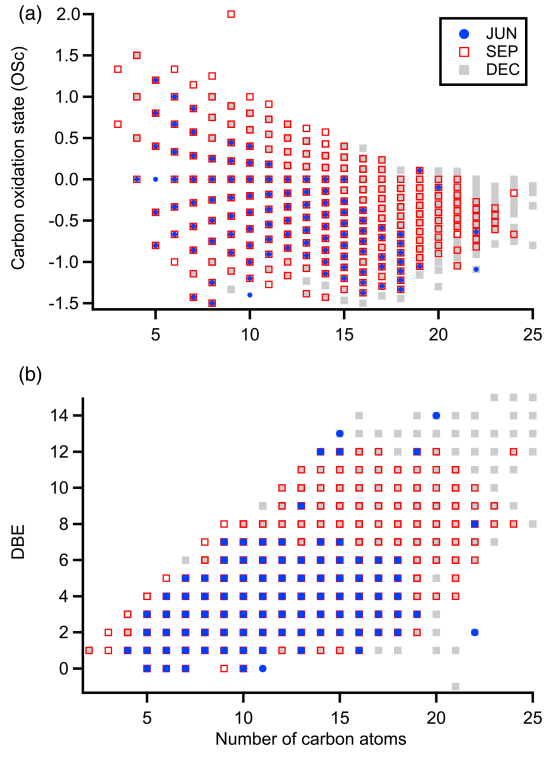

Figure 4. Comparison of **(a)** the carbon oxidation states and **(b)** the double-bond equivalents of CHO-containing molecules observed during each seasonal period.

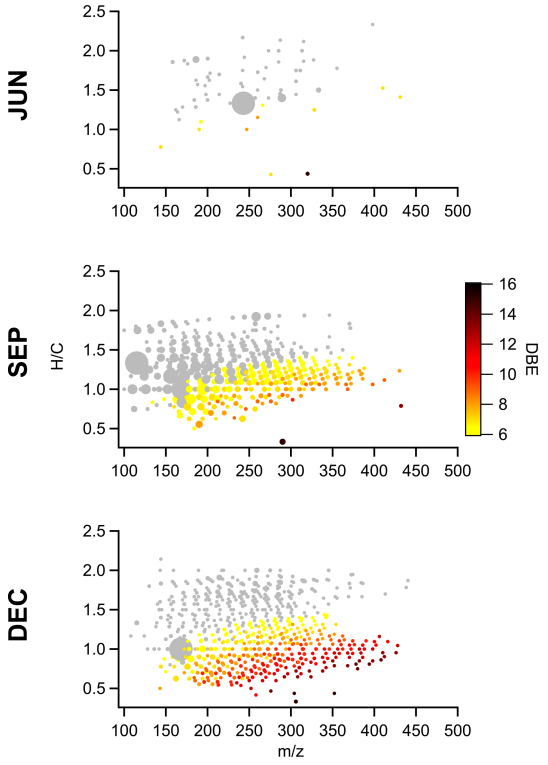

Figure 5. Distributions of double-bond equivalents (DBEs) for CHON-containing molecules observed during each seasonal period. The marker size indicates the relative ion abundance. Molecules with fewer than six DBEs are shown in gray.

ahue et al., 2011). Although these species are most likely not present at the concentrations needed to initiate particle formation at the surface, it should be noted that many species classified as SVOCs or LVOCs at standard temperature and pressure levels (298 K and 1 atm, respectively) are classified as lower-volatility species in the upper atmosphere, where temperatures are much lower. This is consistent with prior observations showing that Amazon UAPs are largely formed in the free troposphere (Zhao et al., 2020). Figure S2 shows particle size distributions recorded at the site from September 2016 through June 2017 (Fig. S2a), as well as the time-averaged distributions for the three seasonal periods (Fig. S2b). No clear NPF events were observed at the surface during any of the periods, though the highest UAP number concentrations were detected during the drier months (late June and September–December). Previous studies (Franco et al., 2022; Varanda Rizzo et al., 2018) have observed a similar seasonal dependence with regard to particle concentrations in central Amazonia, with the dry season being dominated by accumulation-mode particles ($\sim$ 100–600 in diameter), possibly arising from regional biomass-burning events. The average size distributions bear a striking resemblance across the different periods, suggesting that any differences in aerosol molecular properties, including volatility, are not due to the sampled particle size.

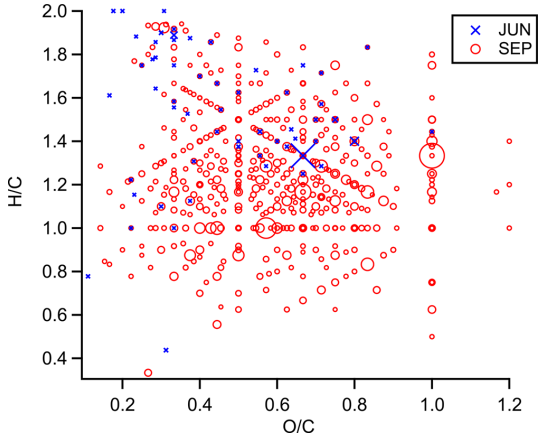

Figure 6. Van Krevelen diagram of the CHON molecules observed in JUN (blue crosses) and SEP (red circles). The marker size indicates the relative ion abundance.

Isoprene organosulfates, including IEPOX-OS ($C_5H_{12}O_7S$; $C_0 = 0.16\,\mu g\,m^{-3}$), dominate the LVOC fraction, particularly in JUN and SEP (Fig. 7). This is consistent with Lopez-Hilfiker et al. (2016), who empirically classified IEPOX SOA components as having low volatility by studying their thermal-desorption characteristics. How-

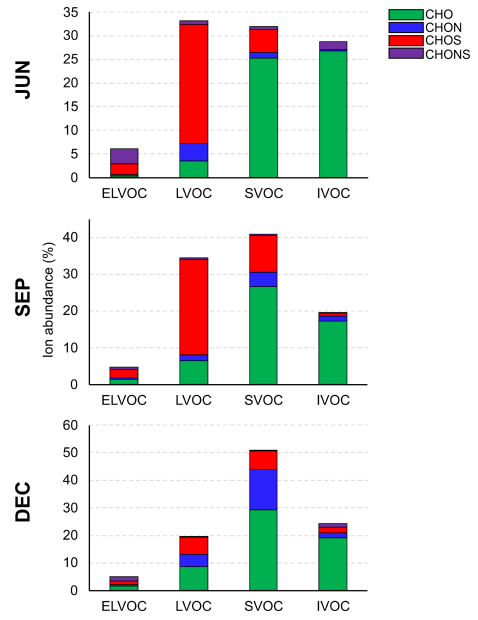

Figure 7. Compound class volatility distributions calculated for the three seasonal periods. Ion abundance (expressed as a percentage) is relative to each sample. IVOC: intermediate-volatility organic compound.

ever, the actual value estimated for C_0 here is several orders of magnitude higher than that estimated by Lopez-Hilfiker et al. (2016). It has been demonstrated previously that the parameterization developed by Li et al. (2016) can significantly overestimate C_0 for certain atmospherically relevant compounds, including nitrogen-containing species (CHON) (Isaacman-VanWertz and Aumont, 2021), likely due to inherent functional-group biases in the training set of molecules used to develop the parameterization. Given that the most abundant CHOS molecule observed here is very likely an organosulfate species (Fig. S3) and that only 17 of the 925 compounds used in the training set from Li et al. (2016) were organosulfates, a similar bias may be observed here. Nevertheless, the low (if not lower) volatility and high relative abundance of isoprene organosulfates observed in this study imply that these species are likely key contributors to UAP growth in the region. In addition to isoprene-derived species, other CHOS molecules likely also contribute significantly as many of the individual species are classified as either LVOCs or extremely low-volatility organic compounds (ELVOCs; $C_0 < 3 \times 10^{-4}$) (Fig. S10). Given that easterly winds were dominant during the sampling periods (Fig. 3a), a key source of sulfate is likely the oxidation of dimethyl sulfide (DMS), given its aforementioned association with marine environments (Andreae and Raemdonck, 1983), which forms methanesulfonic acid and sulfuric acid as secondary products (von Glasow and Crutzen, 2004). The Amazon ecosystem itself has also been identified as another source of DMS, with emissions from plants and soils shown to be strongly dependent on light and temperature (Jardine et al., 2015). In addition to DMS, regional sulfate production – and, thus, UAP growth – is likely highly sensitive to any contributions from SO_2 emission sources, such as biomass burning and fossil fuel combustion on land and at sea (Andreae, 2019; Lee et al., 2011). The abundant biomass-burning-related species, including $C_7H_7O_4N$ ($C_0 = 296\,\mu g\,m^{-3}$) and $C_7H_{12}O_7$ ($C_0 = 7.6\,\mu g\,m^{-3}$), fall into the SVOC fraction, contributing to the dominance of this fraction in DEC. Also contributing to the SVOC fraction are several MT SOA markers, such as MBTCA ($C_8H_{12}O_6$; $C_0 = 94\,\mu g\,m^{-3}$) and C_{9-10} monomer species. It is noteworthy that the C_0 value estimated by Thoma et al. (2022) for MBTCA using the SIMPOL.1 model, which considers the volatility contribution of specific functional groups (including carboxylic acids), is 4 orders of magnitude lower than the estimate used here and, therefore, could be classified as an LVOC. It is reasonable to suspect that other species containing carboxylic acid moieties, particularly those with more than one, may be also overestimated, causing uncertainty in the volatility distributions of each of the compound classes used here, all of which contain oxygen. CHO monomers with $C_{<8}$, associated with most of the monoterpene and isoprene oxidation products identified here, are generally classified here as intermediate-volatility organic compounds (IVOCs; $300 < C_0 < 3 \times 10^6\,\mu g\,m^{-3}$). Though functional-group elucidation may evidence that they have a lower volatility due to the suspected abundance of hydroxyl moieties (Donahue et al., 2011), the PBOA sugar markers are classified here as either SVOC species (glucose and mannitol) or IVOC species (arabitol). In general, the molecular-volatility distributions, taken together with the size distribution data, suggest that the secondary UAPs measured here were likely nucleated elsewhere, such as over the Atlantic Ocean (e.g., sulfuric acid nucleation) or the Amazon free troposphere (e.g., organic vapor nucleation), and that what was sampled mostly comprised aged aerosol components with low to intermediate volatility. At the regional level, UAPs larger than nucleation sizes (> 10 nm in diameter) are also likely contributed by other sources, such as biomass burning in the dry season (SEP and DEC) and biological-spore emissions in the late wet season (JUN).

4 Conclusions

UAPs collected from an eastern Amazon rainforest during three distinct seasonal periods exhibited compositional differences reflecting seasonality in emission sources and aerosol molecular processing. Our observations suggest that isoprene oxidation chemistry is likely a key contributor to UAP composition in the eastern Amazon year-round and that any regional perturbations in isoprene and/or sulfate emission sources could have a significant impact on UAP formation and growth characteristics in the future. Known mark-

ers for biological-spore emissions were tentatively identified in UAPs, with peak abundance observed in the sample from the late wet season (JUN). To the best of our knowledge, this finding provides the first chemical evidence of the influence of primary biogenic sources on UAP composition in the Amazon. To better assess the relative importance of these sources, future measurements are needed to establish the prevalence of spore emission and fragmentation throughout the wet season and in different regions of the Amazon. Secondary emission sources related to the oxidation of isoprene and monoterpenes appear to contribute most to UAP composition during the peak dry season (SEP), aligning with the seasonal peak in VOC emissions and solar radiation. In the late dry season (DEC), biomass burning appears to have a substantial impact on UAP composition, as indicated by the abundance of tentatively identified species, such as methyl-nitrocatechol, and corroborated by MODIS fire anomaly data. Future emission scenarios in which wildfire and agricultural burning events are more frequent could therefore significantly alter regional UAP concentrations and growth characteristics during this time of year. Inasmuch as the Tapajós National Forest is viewed as a model for the future of the Amazon (Cox et al., 2000), our study provides evidence that this source will likely have an increasing influence on UAP emissions in other regions, such as central Amazonia, as well.

Reflecting the differences observed in the distribution of suspected marker species, seasonal changes in the properties of all UAP molecular constituents were also apparent. Compared to those observed in the late wet season, CHO and CHON organics detected in the dry season were more oxidized and unsaturated, suggesting differences in the extent of aerosol processing, such as those pertaining to photochemical aging. Examining the distribution of molecular volatilities reveals that while a strong presence of low-volatility species was found in both the late wet season and the peak dry season due to the abundance of isoprene-derived organosulfates, semivolatile species – likely emitted from biomass burning – dominate the volatility distribution in the late dry season. Although the strong presence of low-volatility organosulfates suggests that many of the sampled UAPs formed via sulfuric acid nucleation occurring to the east of the site, it is unclear whether semivolatile species contributed by biomass burning condensed onto these seeded particles or were emitted and/or formed through a separate mechanism. Similarly, it is unclear what fraction of observed semivolatile BVOC oxidation products contributed to the condensational growth of seeded particles near the surface or nucleated new particles in the upper atmosphere. Future studies on the mixing state of Amazon UAPs would help us more quantitatively understand how the identified emission sources fit into the formation and growth history of new particles in the region. Regardless, it is clear – both from the year-round abundance of sulfated species and the seasonal abundance of biomass-burning markers in UAPs – that human activity is likely already playing a role in such formation and growth processes and will, indeed, probably have a greater influence in the future.

Data availability. Data are publicly available and are archived at https://doi.org/10.5061/dryad.k6djh9wgb (Smith and Thomas, 2024). Meteorological ERA5 reanalysis data from the European Centre for Medium-Range Weather Forecasts (https://doi.org/10.24381/cds.adbb2d47, Hersbach et al., 2023) are publicly available from the Climate Data Store (https://cds.climate.copernicus.eu, last access: 12 June 2024).

Supplement. The supplement related to this article is available online at: https://doi.org/10.5194/acp-25-959-2025-supplement.

Author contributions. JNS and JT secured funding, conceived the research concept, and made on-site measurements. JNS and HSG retrieved samples and analyzed the size distribution data. AET analyzed samples and visualized data under the supervision of JNS. AET prepared the paper with contributions from all authors.

Competing interests. The contact author has declared that none of the authors has any competing interests.

Disclaimer. Publisher's note: Copernicus Publications remains neutral with regard to jurisdictional claims made in the text, published maps, institutional affiliations, or any other geographical representation in this paper. While Copernicus Publications makes every effort to include appropriate place names, the final responsibility lies with the authors.

Acknowledgements. The authors acknowledge funding from the Brazilian Scientific Mobility Program (Ciência sem Fronteiras) Special Visiting Researcher scholarship. Roger Seco acknowledges a Ramón y Cajal grant (grant no. RYC2020-029216-I) funded by the Ministerio de Ciencia e Innovación through the Agencia Estatal de Investigación (MCIN/AEI/10.13039/501100011033) and by the ESF's "Investing in Your Future" initiative. IDAEA-CSIC is a "Severo Ochoa Center of Excellence" project (MCIN/AEI; project no. CEX2018-000794-S). We acknowledge the use of imagery from NASA's Fire Information for Resource Management System (FIRMS) (https://earthdata.nasa.gov/firms, last access: 20 May 2024), part of NASA's Earth Science Data and Information System (ESDIS). James N. Smith acknowledges funding from the US Department of Energy (grant no. DE-SC0012704). The authors thank Véronique Perraud, Deanna C. Myers, Michelia Dam, Paulus S. Bauer, Madeline E. Cooke, Jeremy Wakeen, Anna Kapp, Colleen E. Miller, Kristen L. Kramer, and Berenice Rojas for their contributions to discussions related to this study.

Financial support. This research has been supported by the US Department of Energy's Office of Science (grant no. DE-SC0012704) and the Ministerio de Ciencia e Innovación (grant no. RYC2020-029216-I).

Review statement. This paper was edited by Joachim Curtius and reviewed by Alexander Vogel and one anonymous referee.

References

Allan, J. D., Morgan, W. T., Darbyshire, E., Flynn, M. J., Williams, P. I., Oram, D. E., Artaxo, P., Brito, J., Lee, J. D., and Coe, H.: Airborne observations of IEPOX-derived isoprene SOA in the Amazon during SAMBBA, Atmos. Chem. Phys., 14, 11393–11407, https://doi.org/10.5194/acp-14-11393-2014, 2014.

Allen, J., Oberdorster, G., Morris-Schaffer, K., Wong, C., Klocke, C., Sobolewski, M., Conrad, K., Mayer-Proschel, M., and Cory-Slechta, D.: Developmental neurotoxicity of inhaled ambient ultrafine particle air pollution: Parallels with neuropathological and behavioral features of autism and other neurodevelopmental disorders, NeuroToxicology, 59, 140–154, https://doi.org/10.1016/j.neuro.2015.12.014, 2017.

Alves, E. G., Jardine, K., Tota, J., Jardine, A., Yãnez-Serrano, A. M., Karl, T., Tavares, J., Nelson, B., Gu, D., Stavrakou, T., Martin, S., Artaxo, P., Manzi, A., and Guenther, A.: Seasonality of isoprenoid emissions from a primary rainforest in central Amazonia, Atmos. Chem. Phys., 16, 3903–3925, https://doi.org/10.5194/acp-16-3903-2016, 2016.

Alves, E. G., Taylor, T., Robin, M., Oliveira, D. P., Schietti, J., Júnior, S. D., Zannoni, N., Williams, J., Hartmann, C., Gonçalves, J. F. C., Schöngart, J., Wittmann, F., and Piedade, M. T. F.: Seasonal shifts in isoprenoid emission composition from three hyperdominant tree species in central Amazonia, Plant Biol., 24, 721–733, https://doi.org/10.1111/plb.13419, 2022.

Andreae, M. O.: Emission of trace gases and aerosols from biomass burning – an updated assessment, Atmos. Chem. Phys., 19, 8523–8546, https://doi.org/10.5194/acp-19-8523-2019, 2019.

Andreae, M. O. and Raemdonck, H.: Dimethyl Sulfide in the Surface Ocean and the Marine Atmosphere: A Global View, Science, 221, 744–747, https://doi.org/10.1126/science.221.4612.744, 1983.

Andreae, M. O., Rosenfeld, D., Artaxo, P., Costa, A. A., Frank, G. P., Longo, K. M., and Silva-Dias, M. A. F.: Smoking Rain Clouds over the Amazon, Science, 303, 1337–1342, https://doi.org/10.1126/science.1092779, 2004.

Andreae, M. O., Afchine, A., Albrecht, R., Holanda, B. A., Artaxo, P., Barbosa, H. M. J., Borrmann, S., Cecchini, M. A., Costa, A., Dollner, M., Fütterer, D., Järvinen, E., Jurkat, T., Klimach, T., Konemann, T., Knote, C., Krämer, M., Krisna, T., Machado, L. A. T., Mertes, S., Minikin, A., Pöhlker, C., Pöhlker, M. L., Pöschl, U., Rosenfeld, D., Sauer, D., Schlager, H., Schnaiter, M., Schneider, J., Schulz, C., Spanu, A., Sperling, V. B., Voigt, C., Walser, A., Wang, J., Weinzierl, B., Wendisch, M., and Ziereis, H.: Aerosol characteristics and particle production in the upper troposphere over the Amazon Basin, Atmos. Chem. Phys., 18, 921–961, https://doi.org/10.5194/acp-18-921-2018, 2018.

Andreae, M. O., Andreae, T. W., Ditas, F., and Pöhlker, C.: Frequent new particle formation at remote sites in the subboreal forest of North America, Atmos. Chem. Phys., 22, 2487–2505, https://doi.org/10.5194/acp-22-2487-2022, 2022.

Armstrong, N. C., Chen, Y., Cui, T., Zhang, Y., Christensen, C., Zhang, Z., Turpin, B. J., Chan, M. N., Gold, A., Ault, A. P., and Surratt, J. D.: Isoprene Epoxydiol-Derived Sulfated and Nonsulfated Oligomers Suppress Particulate Mass Loss during Oxidative Aging of Secondary Organic Aerosol, Environ. Sci. Technol., 56, 16611–16620, https://doi.org/10.1021/acs.est.2c03200, 2022.

Aschmann, S. M. and Atkinson, R.: Formation Yields of Methyl Vinyl Ketone and Methacrolein from the Gas-Phase Reaction of O3 with Isoprene, Environ. Sci. Technol., 28, 1539–1542, https://doi.org/10.1021/es00057a025, 1994.

Attygalle, A. B., García-Rubio, S., Ta, J., and Meinwald, J.: Collisionally-induced dissociation mass spectra of organic sulfate anions, Journal of the Chemical Society, Perkin Transactions 2, 498–506 pp., https://doi.org/10.1039/b009019k, 2001.

Baboomian, V. J., Crescenzo, G. V., Huang, Y., Mahrt, F., Shiraiwa, M., Bertram, A. K., and Nizkorodov, S. A.: Sunlight can convert atmospheric aerosols into a glassy solid state and modify their environmental impacts, P. Natl. Acad. Sci. USA, 119, e2208121119, https://doi.org/10.1073/pnas.2208121119, 2022.

Barket, D. J., Grossenbacher, J. W., Hurst, J. M., Shepson, P. B., Olszyna, K., Thornberry, T., Carroll, M. A., Roberts, J., Stroud, C., Bottenheim, J., and Biesenthal, T.: A study of the NO_x dependence of isoprene oxidation, J. Geophys. Res.-Atmos., 109, D11310, https://doi.org/10.1029/2003JD003965, 2004.

Bauer, H., Claeys, M., Vermeylen, R., Schueller, E., Weinke, G., Berger, A., and Puxbaum, H.: Arabitol and mannitol as tracers for the quantification of airborne fungal spores, Atmos. Environ., 42, 588–593, https://doi.org/10.1016/j.atmosenv.2007.10.013, 2008.

Bianchi, F., Kurtén, T., Riva, M., Mohr, C., Rissanen, M. P., Roldin, P., Berndt, T., Crounse, J. D., Wennberg, P. O., Mentel, T. F., Wildt, J., Junninen, H., Jokinen, T., Kulmala, M., Worsnop, D. R., Thornton, J. A., Donahue, N., Kjaergaard, H. G., and Ehn, M.: Highly Oxygenated Organic Molecules (HOM) from Gas-Phase Autoxidation Involving Peroxy Radicals: A Key Contributor to Atmospheric Aerosol, Chemical Reviews, American Chemical Society, https://doi.org/10.1021/acs.chemrev.8b00395, 2019.

Brock, C. A., Hamill, P., Wilson, J. C., Jonsson, H. H., and Chan, K. R.: Particle Formation in the Upper Tropical Troposphere: A Source of Nuclei for the Stratospheric Aerosol, Science, 270, 1650–1653, https://doi.org/10.1126/science.270.5242.1650, 1995.

Calderón-Garcidueñas, L. and Ayala, A.: Air Pollution, Ultrafine Particles, and Your Brain: Are Combustion Nanoparticle Emissions and Engineered Nanoparticles Causing Preventable Fatal Neurodegenerative Diseases and Common Neuropsychiatric Outcomes?, Environ. Sci. Technol., 56, 6847–6856, https://doi.org/10.1021/acs.est.1c04706, 2022.

Chen, Q., Farmer, D. K., Rizzo, L. V., Pauliquevis, T., Kuwata, M., Karl, T. G., Guenther, A., Allan, J. D., Coe, H., Andreae, M. O., Pöschl, U., Jimenez, J. L., Artaxo, P., and Martin, S. T.: Submicron particle mass concentrations and sources in the Amazonian wet season (AMAZE-08), Atmos. Chem. Phys., 15, 3687–3701, https://doi.org/10.5194/acp-15-3687-2015, 2015.

China, S., Wang, B., Weis, J., Rizzo, L., Brito, J., Cirino, G. G., Kovarik, L., Artaxo, P., Gilles, M. K., and Laskin, A.: Rupturing of Biological Spores As a Source of Secondary Particles in Amazonia, Environ. Sci. Technol., 50, 12179–12186, https://doi.org/10.1021/acs.est.6b02896, 2016.

Claeys, M., Graham, B., Vas, G., Wang, W., Vermeylen, R., Pashynska, V., Cafmeyer, J., Guyon, P., Andreae, M. O., Artaxo, P., and Maenhaut, W.: Formation of Secondary Organic Aerosols Through Photooxidation of Isoprene, Science, 303, 1173–1176, https://doi.org/10.1126/science.1092805, 2004.

Claeys, M., Szmigielski, R., Kourtchev, I., der Veken, P. V., Vermeylen, R., Maenhaut, W., Jaoui, M., Kleindienst, T. E., Lewandowski, M., Offenberg, J. H., and Edney, E. O.: Hydroxydicarboxylic Acids: Markers for Secondary Organic Aerosol from the Photooxidation of α-Pinene, Environ. Sci. Technol., 41, 1628–1634, https://doi.org/10.1021/es0620181, 2007.

Cox, P. M., Betts, R. A., Jones, C. D., Spall, S. A., and Totterdell, I. J.: Acceleration of global warming due to carbon-cycle feedbacks in a coupled climate model, Nature, 408, 184–187, https://doi.org/10.1038/35041539, 2000.

da Rocha, H. R., Manzi, A. O., Cabral, O. M., Miller, S. D., Goulden, M. L., Saleska, S. R., R.-Coupe, N., Wofsy, S. C., Borma, L. S., Artaxo, P., Vourlitis, G., Nogueira, J. S., Cardoso, F. L., Nobre, A. D., Kruijt, B., Freitas, H. C., von Randow, C., Aguiar, R. G., and Maia, J. F.: Patterns of water and heat flux across a biome gradient from tropical forest to savanna in Brazil, J. Geophys. Res.-Biogeosci., 114, 1–8, https://doi.org/10.1029/2007JG000640, 2009.

Dada, L., Chellapermal, R., Buenrostro Mazon, S., Paasonen, P., Lampilahti, J., Manninen, H. E., Junninen, H., Petäjä, T., Kerminen, V.-M., and Kulmala, M.: Refined classification and characterization of atmospheric new-particle formation events using air ions, Atmos. Chem. Phys., 18, 17883–17893, https://doi.org/10.5194/acp-18-17883-2018, 2018.

Dal Maso, M., Sogacheva, L., Anisimov, M. P., Arshinov, M., Baklanov, A., Belan, B., Khodzer, T. V., Obolkin, V. A., Staroverova, A., Vlasov, A., Zagaynov, V. A., Lushnikov, A., Lyubovtseva, Y. S., Riipinen, I., Kerminen, V.-M., and Kulmala, M.: Aerosol particle formation events at two Siberian stations inside the boreal forest, Boreal Environ. Res., 13, 81–92, 2008.

de Sá, S. S., Rizzo, L. V., Palm, B. B., Campuzano-Jost, P., Day, D. A., Yee, L. D., Wernis, R., Isaacman-VanWertz, G., Brito, J., Carbone, S., Liu, Y. J., Sedlacek, A., Springston, S., Goldstein, A. H., Barbosa, H. M. J., Alexander, M. L., Artaxo, P., Jimenez, J. L., and Martin, S. T.: Contributions of biomass-burning, urban, and biogenic emissions to the concentrations and light-absorbing properties of particulate matter in central Amazonia during the dry season, Atmos. Chem. Phys., 19, 7973–8001, https://doi.org/10.5194/acp-19-7973-2019, 2019.

Donahue, N. M., Epstein, S. A., Pandis, S. N., and Robinson, A. L.: A two-dimensional volatility basis set: 1. organic-aerosol mixing thermodynamics, Atmos. Chem. Phys., 11, 3303–3318, https://doi.org/10.5194/acp-11-3303-2011, 2011.

Dunne, E. M., Gordon, H., Kürten, A., Almeida, J., Duplissy, J., Williamson, C., Ortega, I. K., Pringle, K. J., Adamov, A., Baltensperger, U., Barmet, P., Benduhn, F., Bianchi, F., Breitenlechner, M., Clarke, A., Curtius, J., Dommen, J., Donahue, N. M., Ehrhart, S., Flagan, R. C., Franchin, A., Guida, R., Hakala, J., Hansel, A., Heinritzi, M., Jokinen, T., Kangasluoma, J., Kirkby, J., Kulmala, M., Kupc, A., Lawler, M. J., Lehtipalo, K., Makhmutov, V., Mann, G., Mathot, S., Merikanto, J., Miettinen, P., Nenes, A., Onnela, A., Rap, A., Reddington, C. L. S., Riccobono, F., Richards, N. A. D., Rissanen, M. P., Rondo, L., Sarnela, N., Schobesberger, S., Sengupta, K., Simon, M., Sipilä, M., Smith, J. N., Stozkhov, Y., Tomé, A., Tröstl, J., Wagner, P. E., Wimmer, D., Winkler, P. M., Worsnop, D. R., and Carslaw, K. S.: Global atmospheric particle formation from CERN CLOUD measurements, Science, 354, 1119–1124, https://doi.org/10.1126/science.aaf2649, 2016.

Ehn, M., Thornton, J. A., Kleist, E., Sipilä, M., Junninen, H., Pullinen, I., Springer, M., Rubach, F., Tillmann, R., Lee, B., Lopez-Hilfiker, F., Andres, S., Acir, I.-H., Rissanen, M., Jokinen, T., Schobesberger, S., Kangasluoma, J., Kontkanen, J., Nieminen, T., Kurtén, T., Nielsen, L. B., Jørgensen, S., Kjaergaard, H. G., Canagaratna, M., Maso, M. D., Berndt, T., Petäjä, T., Wahner, A., Kerminen, V.-M., Kulmala, M., Worsnop, D. R., Wildt, J., and Mentel, T. F.: A large source of low-volatility secondary organic aerosol, Nature, 506, 476–479, https://doi.org/10.1038/nature13032, 2014.

Ekman, A. M. L., Krejci, R., Engström, A., Ström, J., de Reus, M., Williams, J., and Andreae, M. O.: Do organics contribute to small particle formation in the Amazonian upper troposphere?, Geophys. Res. Lett., 35, L17810, https://doi.org/10.1029/2008GL034970, 2008.

Fan, J., Rosenfeld, D., Zhang, Y., Giangrande, S. E., Li, Z., Machado, L. A. T., Martin, S. T., Yang, Y., Wang, J., Artaxo, P., Barbosa, H. M. J., Braga, R. C., Comstock, J. M., Feng, Z., Gao, W., Gomes, H. B., Mei, F., Pöhlker, C., Pöhlker, M. L., Pöschl, U., and de Souza, R. A. F.: Substantial convection and precipitation enhancements by ultrafineaerosol particles, Science, 359, 411–418, https://doi.org/10.1126/science.aan8461, 2018.

Fernandez, A. E., Lewis, G. S., and Hering, S. V.: Design and Laboratory Evaluation of a Sequential Spot Sampler for Time-Resolved Measurement of Airborne Particle Composition, Aerosol Sci. Technol., 48, 655–663, https://doi.org/10.1080/02786826.2014.911409, 2014.

Flores, B. M., Montoya, E., Sakschewski, B., Nascimento, N., Staal, A., Betts, R. A., Levis, C., Lapola, D. M., Esquível-Muelbert, A., Jakovac, C., Nobre, C. A., Oliveira, R. S., Borma, L. S., Nian, D., Boers, N., Hecht, S. B., ter Steege, H., Arieira, J., Lucas, I. L., Berenguer, E., Marengo, J. A., Gatti, L. V., Mattos, C. R. C., and Hirota, M.: Critical transitions in the Amazon forest system, Nature, 626, 555–564, https://doi.org/10.1038/s41586-023-06970-0, 2024.

Franco, M. A., Ditas, F., Kremper, L. A., Machado, L. A. T., Andreae, M. O., Araújo, A., Barbosa, H. M. J., de Brito, J. F., Carbone, S., Holanda, B. A., Morais, F. G., Nascimento, J. P., Pöhlker, M. L., Rizzo, L. V., Sá, M., Saturno, J., Walter, D., Wolff, S., Pöschl, U., Artaxo, P., and Pöhlker, C.: Occurrence and growth of sub-50 nm aerosol particles in the Amazonian boundary layer, Atmos. Chem. Phys., 22, 3469–3492, https://doi.org/10.5194/acp-22-3469-2022, 2022.

Giglio, L., Boschetti, L., Roy, D. P., Humber, M. L., and Justice, C. O.: The Collection 6 MODIS burned area mapping algorithm and product, Remote Sens. Environ., 217, 72–85, https://doi.org/10.1016/j.rse.2018.08.005, 2018.

Glasius, M., Bering, M. S., Yee, L. D., de Sá, S. S., Isaacman-VanWertz, G., Wernis, R. A., Barbosa, H. M. J., Alexander,

M. L., Palm, B. B., Hu, W., Campuzano-Jost, P., Day, D. A., Jimenez, J. L., Shrivastava, M., Martin, S. T., and Goldstein, A. H.: Organosulfates in aerosols downwind of an urban region in central Amazon, Environ. Sci.-Process. Impacts, 20, 1546–1558, https://doi.org/10.1039/C8EM00413G, 2018.

Glicker, H. S., Lawler, M. J., Ortega, J., de Sá, S. S., Martin, S. T., Artaxo, P., Vega Bustillos, O., de Souza, R., Tota, J., Carlton, A., and Smith, J. N.: Chemical composition of ultrafine aerosol particles in central Amazonia during the wet season, Atmos. Chem. Phys., 19, 13053–13066, https://doi.org/10.5194/acp-19-13053-2019, 2019.

Go, B. R., Lyu, Y., Ji, Y., Li, Y. J., Huang, D. D., Li, X., Nah, T., Lam, C. H., and Chan, C. K.: Aqueous secondary organic aerosol formation from the direct photosensitized oxidation of vanillin in the absence and presence of ammonium nitrate, Atmos. Chem. Phys., 22, 273–293, https://doi.org/10.5194/acp-22-273-2022, 2022.

Gordon, H., Kirkby, J., Baltensperger, U., Bianchi, F., Breitenlechner, M., Curtius, J., Dias, A., Dommen, J., Donahue, N. M., Dunne, E. M., Duplissy, J., Ehrhart, S., Flagan, R. C., Frege, C., Fuchs, C., Hansel, A., Hoyle, C. R., Kulmala, M., Kürten, A., Lehtipalo, K., Makhmutov, V., Molteni, U., Rissanen, M. P., Stozkhov, Y., Tröstl, J., Tsagkogeorgas, G., Wagner, R., Williamson, C., Wimmer, D., Winkler, P. M., Yan, C., and Carslaw, K. S.: Causes and importance of new particle formation in the present-day and preindustrial atmospheres, J. Geophys. Res.-Atmos., 122, 8739–8760, https://doi.org/10.1002/2017JD026844, 2017.

Guenther, A. B., Jiang, X., Heald, C. L., Sakulyanontvittaya, T., Duhl, T., Emmons, L. K., and Wang, X.: The Model of Emissions of Gases and Aerosols from Nature version 2.1 (MEGAN2.1): an extended and updated framework for modeling biogenic emissions, Geosci. Model Dev., 5, 1471–1492, https://doi.org/10.5194/gmd-5-1471-2012, 2012.

Hersbach, H., Bell, B., Berrisford, P., Biavati, G., Horányi, A., Muñoz Sabater, J., Nicolas, J., Peubey, C., Radu, R., Rozum, I., Schepers, D., Simmons, A., Soci, C., Dee, D., and Thépaut, J.-N.: ERA5 hourly data on single levels from 1940 to present, Copernicus Climate Change Service (C3S) Climate Data Store (CDS) [data set], https://doi.org/10.24381/cds.adbb2d47, 2023.

Hodshire, A. L., Palm, B. B., Alexander, M. L., Bian, Q., Campuzano-Jost, P., Cross, E. S., Day, D. A., de Sá, S. S., Guenther, A. B., Hansel, A., Hunter, J. F., Jud, W., Karl, T., Kim, S., Kroll, J. H., Park, J.-H., Peng, Z., Seco, R., Smith, J. N., Jimenez, J. L., and Pierce, J. R.: Constraining nucleation, condensation, and chemistry in oxidation flow reactors using size-distribution measurements and aerosol microphysical modeling, Atmos. Chem. Phys., 18, 12433–12460, https://doi.org/10.5194/acp-18-12433-2018, 2018.

Huffman, J. A., Prenni, A. J., DeMott, P. J., Pöhlker, C., Mason, R. H., Robinson, N. H., Fröhlich-Nowoisky, J., Tobo, Y., Després, V. R., Garcia, E., Gochis, D. J., Harris, E., Müller-Germann, I., Ruzene, C., Schmer, B., Sinha, B., Day, D. A., Andreae, M. O., Jimenez, J. L., Gallagher, M., Kreidenweis, S. M., Bertram, A. K., and Pöschl, U.: High concentrations of biological aerosol particles and ice nuclei during and after rain, Atmos. Chem. Phys., 13, 6151–6164, https://doi.org/10.5194/acp-13-6151-2013, 2013.

Iinuma, Y., Böge, O., Gräfe, R., and Herrmann, H.: Methyl-Nitrocatechols: Atmospheric Tracer Compounds for Biomass Burning Secondary Organic Aerosols, Environ. Sci. Technol., 44, 8453–8459, https://doi.org/10.1021/es102938a, 2010.

Isaacman-VanWertz, G. and Aumont, B.: Impact of organic molecular structure on the estimation of atmospherically relevant physicochemical parameters, Atmos. Chem. Phys., 21, 6541–6563, https://doi.org/10.5194/acp-21-6541-2021, 2021.

Isaacman-VanWertz, G., Yee, L. D., Kreisberg, N. M., Wernis, R., Moss, J. A., Hering, S. V., de Sá, S. S., Martin, S. T., Alexander, M. L., Palm, B. B., Hu, W., Campuzano-Jost, P., Day, D. A., Jimenez, J. L., Riva, M., Surratt, J. D., Viegas, J., Manzi, A., Edgerton, E., Baumann, K., Souza, R., Artaxo, P., and Goldstein, A. H.: Ambient Gas-Particle Partitioning of Tracers for Biogenic Oxidation, Environ. Sci. Technol., 50, 9952–9962, https://doi.org/10.1021/acs.est.6b01674, 2016.

Jaitly, N., Mayampurath, A., Littlefield, K., Adkins, J. N., Anderson, G. A., and Smith, R. D.: Decon2LS: An open-source software package for automated processing and visualization of high resolution mass spectrometry data, BMC Bioinformatics, 10, 87, https://doi.org/10.1186/1471-2105-10-87, 2009.

Jaoui, M., Szmigielski, R., Nestorowicz, K., Kolodziejczyk, A., Sarang, K., Rudzinski, K. J., Konopka, A., Bulska, E., Lewandowski, M., and Kleindienst, T. E.: Organic Hydroxy Acids as Highly Oxygenated Molecular (HOM) Tracers for Aged Isoprene Aerosol, Environ. Sci. Technol., 53, 14516–14527, https://doi.org/10.1021/acs.est.9b05075, 2019.

Jardine, K., Yañez-Serrano, A. M., Williams, J., Kunert, N., Jardine, A., Taylor, T., Abrell, L., Artaxo, P., Guenther, A., Hewitt, C. N., House, E., Florentino, A. P., Manzi, A., Higuchi, N., Kesselmeier, J., Behrendt, T., Veres, P. R., Derstroff, B., Fuentes, J. D., Martin, S. T., and Andreae, M. O.: Dimethyl sulfide in the Amazon rain forest, Global Biogeochem. Cy., 29, 19–32, https://doi.org/10.1002/2014GB004969, 2015.

Jenkins, B. M., Jones, A. D., Turn, S. Q., and Williams, R. B.: Emission Factors for Polycyclic Aromatic Hydrocarbons from Biomass Burning, Environ. Sci. Technol., 30, 2462–2469, https://doi.org/10.1021/es950699m, 1996.

Jiang, H., Carena, L., He, Y., Wang, Y., Zhou, W., Yang, L., Luan, T., Li, X., Brigante, M., Vione, D., and Gligorovski, S.: Photosensitized Degradation of DMSO Initiated by PAHs at the Air-Water Interface, as an Alternative Source of Organic Sulfur Compounds to the Atmosphere, J. Geophys. Res.-Atmos., 126, e2021JD035346, https://doi.org/10.1029/2021JD035346, 2021.

Jiang, H., He, Y., Wang, Y., Li, S., Jiang, B., Carena, L., Li, X., Yang, L., Luan, T., Vione, D., and Gligorovski, S.: Formation of organic sulfur compounds through SO2-initiated photochemistry of PAHs and dimethylsulfoxide at the air-water interface, Atmos. Chem. Phys., 22, 4237–4252, https://doi.org/10.5194/acp-22-4237-2022, 2022.

Kahnt, A., Iinuma, Y., Blockhuys, F., Mutzel, A., Vermeylen, R., Kleindienst, T. E., Jaoui, M., Offenberg, J. H., Lewandowski, M., Böge, O., Herrmann, H., Maenhaut, W., and Claeys, M.: 2-Hydroxyterpenylic Acid: An Oxygenated Marker Compound for α-Pinene Secondary Organic Aerosol in Ambient Fine Aerosol, Environ. Sci. Technol., 48, 4901–4908, https://doi.org/10.1021/es500377d, 2014.

Karl, T. G., Christian, T. J., Yokelson, R. J., Artaxo, P., Hao, W. M., and Guenther, A.: The Tropical Forest and Fire Emis-

sions Experiment: method evaluation of volatile organic compound emissions measured by PTR-MS, FTIR, and GC from tropical biomass burning, Atmos. Chem. Phys., 7, 5883–5897, https://doi.org/10.5194/acp-7-5883-2007, 2007.

Kong, X., Salvador, C. M., Carlsson, S., Pathak, R., Davidsson, K. O., Breton, M. L., Gaita, S. M., Mitra, K., Åsa M. Hallquist, Hallquist, M., and Pettersson, J. B.: Molecular characterization and optical properties of primary emissions from a residential wood burning boiler, Sci. Total Environ., 754, 142143, https://doi.org/10.1016/j.scitotenv.2020.142143, 2021.

Kourtchev, I., Godoi, R. H. M., Connors, S., Levine, J. G., Archibald, A. T., Godoi, A. F. L., Paralovo, S. L., Barbosa, C. G. G., Souza, R. A. F., Manzi, A. O., Seco, R., Sjostedt, S., Park, J.-H., Guenther, A., Kim, S., Smith, J., Martin, S. T., and Kalberer, M.: Molecular composition of organic aerosols in central Amazonia: an ultra-high-resolution mass spectrometry study, Atmos. Chem. Phys., 16, 11899–11913, https://doi.org/10.5194/acp-16-11899-2016, 2016.

Kourtchev, I., Szeto, P., O'Connor, I., Popoola, O. A. M., Maenhaut, W., Wenger, J., and Kalberer, M.: Comparison of Heated Electrospray Ionization and Nanoelectrospray Ionization Sources Coupled to Ultra-High-Resolution Mass Spectrometry for Analysis of Highly Complex Atmospheric Aerosol Samples, Anal. Chem., 92, 8396–8403, https://doi.org/10.1021/acs.analchem.0c00971, 2020.

Krechmer, J. E., Coggon, M. M., Massoli, P., Nguyen, T. B., Crounse, J. D., Hu, W., Day, D. A., Tyndall, G. S., Henze, D. K., Rivera-Rios, J. C., Nowak, J. B., Kimmel, J. R., Mauldin, R. L., Stark, H., Jayne, J. T., Sipilä, M., Junninen, H., Clair, J. M. S., Zhang, X., Feiner, P. A., Zhang, L., Miller, D. O., Brune, W. H., Keutsch, F. N., Wennberg, P. O., Seinfeld, J. H., Worsnop, D. R., Jimenez, J. L., and Canagaratna, M. R.: Formation of Low Volatility Organic Compounds and Secondary Organic Aerosol from Isoprene Hydroxyhydroperoxide Low-NO Oxidation, Environ. Sci. Technol., 49, 10330–10339, https://doi.org/10.1021/acs.est.5b02031, 2015.

Kroll, J. H., Donahue, N. M., Jimenez, J. L., Kessler, S. H., Canagaratna, M. R., Wilson, K. R., Altieri, K. E., Mazzoleni, L. R., Wozniak, A. S., Bluhm, H., Mysak, E. R., Smith, J. D., Kolb, C. E., and Worsnop, D. R.: Carbon oxidation state as a metric for describing the chemistry of atmospheric organic aerosol, Nat. Chem., 3, 133–139, https://doi.org/10.1038/nchem.948, 2011.

Kuang, B. Y., Lin, P., Hu, M., and Yu, J. Z.: Aerosol size distribution characteristics of organosulfates in the Pearl River Delta region, China, Atmos. Environ., 130, 23–35, https://doi.org/10.1016/j.atmosenv.2015.09.024, 2016.

Kubátová, A., Vermeylen, R., Claeys, M., Cafmeyer, J., Maenhaut, W., Roberts, G., and Artaxo, P.: Carbonaceous aerosol characterization in the Amazon basin, Brazil: novel dicarboxylic acids and related compounds, Atmos. Environ., 34, 5037–5051, https://doi.org/10.1016/S1352-2310(00)00320-4, 2000.

Langford, B., House, E., Valach, A., Hewitt, C. N., Artaxo, P., Barkley, M. P., Brito, J., Carnell, E., Davison, B., MacKenzie, A. R., Marais, E. A., Newland, M. J., Rickard, A. R., Shaw, M. D., Yáñez-Serrano, A. M., and Nemitz, E.: Seasonality of isoprene emissions and oxidation products above the remote Amazon, Environ. Sci.-Atmos., 2, 230–240, https://doi.org/10.1039/D1EA00057H, 2022.

Lawler, M. J., Draper, D. C., and Smith, J. N.: Atmospheric fungal nanoparticle bursts, Sci. Adv., 6, eaar2547, https://doi.org/10.1126/sciadv.aax9051, 2020.

Lawson, D. R. and Winchester, J. W.: Sulfur, potassium, and phosphorus associations in aerosols from South American tropical rain forests, J. Geophys. Res.-Oceans, 84, 3723–3727, https://doi.org/10.1029/JC084iC07p03723, 1979.

Lee, C., Martin, R. V., van Donkelaar, A., Lee, H., Dickerson, R. R., Hains, J. C., Krotkov, N., Richter, A., Vinnikov, K., and Schwab, J. J.: SO_2 emissions and lifetimes: Estimates from inverse modeling using in situ and global, space-based (SCIAMACHY and OMI) observations, J. Geophys. Res., 116, D06304, https://doi.org/10.1029/2010JD014758, 2011.

Leppla, D., Zannoni, N., Kremper, L., Williams, J., Pöhlker, C., Sá, M., Solci, M. C., and Hoffmann, T.: Varying chiral ratio of pinic acid enantiomers above the Amazon rainforest, Atmos. Chem. Phys., 23, 809–820, https://doi.org/10.5194/acp-23-809-2023, 2023.

Lewis, D. H. and Smith, D. C.: Sugar Alcohols (Polyols) in Fungi and Green Plants. I. Distribution, Physiology and Metabolism, The New Phytologist, 66, 143–184, http://www.jstor.org/stable/2430328 (last access: 12 June 2024), 1967.

Li, H., Xu, D., Li, H., Wu, Y., Cheng, Y., Chen, Z., Yin, G., Wang, W., Ge, Y., Niu, Y., Liu, C., Cai, J., Kan, H., Yu, D., and Chen, R.: Exposure to ultrafine particles and oral flora, respiratory function, and biomarkers of inflammation: A panel study in children, Environ. Pollut., 273, 116489, https://doi.org/10.1016/j.envpol.2021.116489, 2021.

Li, Y., Pöschl, U., and Shiraiwa, M.: Molecular corridors and parameterizations of volatility in the chemical evolution of organic aerosols, Atmos. Chem. Phys., 16, 3327–3344, https://doi.org/10.5194/acp-16-3327-2016, 2016.

Liao, J., Froyd, K. D., Murphy, D. M., Keutsch, F. N., Yu, G., Wennberg, P. O., Clair, J. M. S., Crounse, J. D., Wisthaler, A., Mikoviny, T., Jimenez, J. L., Campuzano-Jost, P., Day, D. A., Hu, W., Ryerson, T. B., Pollack, I. B., Peischl, J., Anderson, B. E., Ziemba, L. D., Blake, D. R., Meinardi, S., and Diskin, G.: Airborne measurements of organosulfates over the continental U.S., J. Geophys. Res.-Atmos., 120, 2990–3005, https://doi.org/10.1002/2014JD022378, 2015.

Liu, B. Y. H., Pui, D. Y. H., and Lin, B. Y.: Aerosol Charge Neutralization by a Radioactive Alpha Source, Part. Part. Syst. Char., 3, 111–116, https://doi.org/10.1002/ppsc.19860030304, 1986.

Liu, J., D'Ambro, E. L., Lee, B. H., Lopez-Hilfiker, F. D., Zaveri, R. A., Rivera-Rios, J. C., Keutsch, F. N., Iyer, S., Kurten, T., Zhang, Z., Gold, A., Surratt, J. D., Shilling, J. E., and Thornton, J. A.: Efficient Isoprene Secondary Organic Aerosol Formation from a Non-IEPOX Pathway, Environ. Sci. Technol., 50, 9872–9880, https://doi.org/10.1021/acs.est.6b01872, 2016.

Liu, Y., Brito, J., Dorris, M. R., Rivera-Rios, J. C., Seco, R., Bates, K. H., Artaxo, P., Duvoisin, S., Keutsch, F. N., Kim, S., Goldstein, A. H., Guenther, A. B., Manzi, A. O., Souza, R. A. F., Springston, S. R., Watson, T. B., McKinney, K. A., and Martin, S. T.: Isoprene photochemistry over the Amazon rainforest, P. Natl. Acad. Sci. USA, 113, 6125–6130, https://doi.org/10.1073/pnas.1524136113, 2016.

Liu, Y., Seco, R., Kim, S., Guenther, A. B., Goldstein, A. H., Keutsch, F. N., Springston, S. R., Watson, T. B., Artaxo, P., Souza, R. A. F., McKinney, K. A., and Martin, S. T.: Iso-

prene photo-oxidation products quantify the effect of pollution on hydroxyl radicals over Amazonia, Sci. Adv., 4, eaar2547, https://doi.org/10.1126/sciadv.aar2547, 2018.

Liu, Y. J., Herdlinger-Blatt, I., McKinney, K. A., and Martin, S. T.: Production of methyl vinyl ketone and methacrolein via the hydroperoxyl pathway of isoprene oxidation, Atmos. Chem. Phys., 13, 5715–5730, https://doi.org/10.5194/acp-13-5715-2013, 2013.

Lopez-Hilfiker, F. D., Mohr, C., D'Ambro, E. L., Lutz, A., Riedel, T. P., Gaston, C. J., Iyer, S., Zhang, Z., Gold, A., Surratt, J. D., Lee, B. H., Kurten, T., Hu, W., Jimenez, J., Hallquist, M., and Thornton, J. A.: Molecular Composition and Volatility of Organic Aerosol in the Southeastern U.S.: Implications for IEPOX Derived SOA, Environ. Sci. Technol., 50, 2200–2209, https://doi.org/10.1021/acs.est.5b04769, 2016.

Maclean, A. M., Smith, N. R., Li, Y., Huang, Y., Hettiyadura, A. P. S., Crescenzo, G. V., Shiraiwa, M., Laskin, A., Nizkorodov, S. A., and Bertram, A. K.: Humidity-Dependent Viscosity of Secondary Organic Aerosol from Ozonolysis of β-Caryophyllene: Measurements, Predictions, and Implications, ACS Earth Space Chem., 5, 305–318, https://doi.org/10.1021/acsearthspacechem.0c00296, 2021.

Martin, S. T., Andreae, M. O., Artaxo, P., Baumgardner, D., Chen, Q., Goldstein, A. H., Guenther, A., Heald, C. L., Mayol-Bracero, O. L., McMurry, P. H., Pauliquevis, T., Pöschl, U., Prather, K. A., Roberts, G. C., Saleska, S. R., Dias, M. A. S., Spracklen, D. V., Swietlicki, E., and Trebs, I.: Sources and properties of Amazonian aerosol particles, Rev. Geophys., 48, RG2002, https://doi.org/10.1029/2008RG000280, 2010.

Meinardi, S., Simpson, I. J., Blake, N. J., Blake, D. R., and Rowland, F. S.: Dimethyl disulfide (DMDS) and dimethyl sulfide (DMS) emissions from biomass burning in Australia, Geophys. Res. Lett., 30, 1454, https://doi.org/10.1029/2003GL016967, 2003.

Merikanto, J., Spracklen, D. V., Mann, G. W., Pickering, S. J., and Carslaw, K. S.: Impact of nucleation on global CCN, Atmos. Chem. Phys., 9, 8601–8616, https://doi.org/10.5194/acp-9-8601-2009, 2009.

Murphy, B. N., Donahue, N. M., Robinson, A. L., and Pandis, S. N.: A naming convention for atmospheric organic aerosol, Atmos. Chem. Phys., 14, 5825–5839, https://doi.org/10.5194/acp-14-5825-2014, 2014.

Nassan, F. L., Wang, C., Kelly, R. S., Lasky-Su, J. A., Vokonas, P. S., Koutrakis, P., and Schwartz, J. D.: Ambient PM2.5 species and ultrafine particle exposure and their differential metabolomic signatures, Environ. Int., 151, 106447, https://doi.org/10.1016/j.envint.2021.106447, 2021.

Nguyen, T. B., Bates, K. H., Crounse, J. D., Schwantes, R. H., Zhang, X., Kjaergaard, H. G., Surratt, J. D., Lin, P., Laskin, A., Seinfeld, J. H., and Wennberg, P. O.: Mechanism of the hydroxyl radical oxidation of methacryloyl peroxynitrate (MPAN) and its pathway toward secondary organic aerosol formation in the atmosphere, Phys. Chem. Chem. Phys., 17, 17914–17926, https://doi.org/10.1039/C5CP02001H, 2015.

Nirmalkar, J., Deb, M. K., Tsai, Y. I., and Deshmukh, D. K.: Arabitol and Mannitol as Tracer for Fungal Contribution to Size-Differentiated Particulate Matter of Rural Atmospheric Aerosols, Int. J. Environ. Sci. Develop., 6, 460–463, https://doi.org/10.7763/IJESD.2015.V6.637, 2015.

Nizkorodov, S. A., Laskin, J., and Laskin, A.: Molecular chemistry of organic aerosols through the application of high resolution mass spectrometry, Phys. Chem. Chem. Phys., 13, 3612–3629, https://doi.org/10.1039/c0cp02032j, 2011.

Nölscher, A. C., Yañez-Serrano, A. M., Wolff, S., de Araujo, A. C., Lavrič, J. V., Kesselmeier, J., and Williams, J.: Unexpected seasonality in quantity and composition of Amazon rainforest air reactivity, Nat. Commun., 7, 10383, https://doi.org/10.1038/ncomms10383, 2016.

Olsen, J. V., Macek, B., Lange, O., Makarov, A., Horning, S., and Mann, M.: Higher-energy C-trap dissociation for peptide modification analysis, Nat. Method., 4, 709–712, https://doi.org/10.1038/nmeth1060, 2007.

Palm, B. B., de Sá, S. S., Day, D. A., Campuzano-Jost, P., Hu, W., Seco, R., Sjostedt, S. J., Park, J.-H., Guenther, A. B., Kim, S., Brito, J., Wurm, F., Artaxo, P., Thalman, R., Wang, J., Yee, L. D., Wernis, R., Isaacman-VanWertz, G., Goldstein, A. H., Liu, Y., Springston, S. R., Souza, R., Newburn, M. K., Alexander, M. L., Martin, S. T., and Jimenez, J. L.: Secondary organic aerosol formation from ambient air in an oxidation flow reactor in central Amazonia, Atmos. Chem. Phys., 18, 467–493, https://doi.org/10.5194/acp-18-467-2018, 2018.

Paulot, F., Crounse, J. D., Kjaergaard, H. G., Kürten, A., Clair, J. M. S., Seinfeld, J. H., and Wennberg, P. O.: Unexpected Epoxide Formation in the Gas-Phase Photooxidation of Isoprene, Science, 325, 730–733, https://doi.org/10.1126/science.1172910, 2009.

Pfannerstill, E. Y., Reijrink, N. G., Edtbauer, A., Ringsdorf, A., Zannoni, N., Araújo, A., Ditas, F., Holanda, B. A., Sá, M. O., Tsokankunku, A., Walter, D., Wolff, S., Lavrič, J. V., Pöhlker, C., Sörgel, M., and Williams, J.: Total OH reactivity over the Amazon rainforest: variability with temperature, wind, rain, altitude, time of day, season, and an overall budget closure, Atmos. Chem. Phys., 21, 6231–6256, https://doi.org/10.5194/acp-21-6231-2021, 2021.

Pöhlker, C., Wiedemann, K. T., Sinha, B., Shiraiwa, M., Gunthe, S. S., Smith, M., Su, H., Artaxo, P., Chen, Q., Cheng, Y., Elbert, W., Gilles, M. K., Kilcoyne, A. L. D., Moffet, R. C., Weigand, M., Martin, S. T., Pöschl, U., and Andreae, M. O.: Biogenic Potassium Salt Particles as Seeds for Secondary Organic Aerosol in the Amazon, Science, 337, 1075–1078, https://doi.org/10.1126/science.1223264, 2012.

Reis, G., Souza, S., Neto, H., Branches, R., Silva, R., Peres, L., Pinheiro, D., Lamy, K., Bencherif, H., and Portafaix, T.: Solar Ultraviolet Radiation Temporal Variability Analysis from 2-Year of Continuous Observation in an Amazonian City of Brazil, Atmosphere, 13, 1054, https://doi.org/10.3390/atmos13071054, 2022.

Ren, Y., Shen, G., Shen, H., Zhong, Q., Xu, H., Meng, W., Zhang, W., Yu, X., Yun, X., Luo, Z., Chen, Y., Li, B., Cheng, H., Zhu, D., and Tao, S.: Contributions of biomass burning to global and regional SO_2 emissions, Atmos. Res., 260, 105709, https://doi.org/10.1016/j.atmosres.2021.105709, 2021.

Rickly, P. S., Guo, H., Campuzano-Jost, P., Jimenez, J. L., Wolfe, G. M., Bennett, R., Bourgeois, I., Crounse, J. D., Dibb, J. E., DiGangi, J. P., Diskin, G. S., Dollner, M., Gargulinski, E. M., Hall, S. R., Halliday, H. S., Hanisco, T. F., Hannun, R. A., Liao, J., Moore, R., Nault, B. A., Nowak, J. B., Peischl, J., Robinson, C. E., Ryerson, T., Sanchez, K. J., Schöberl, M., Soja, A. J., St. Clair, J. M., Thornhill, K. L., Ullmann, K., Wennberg, P. O., Weinzierl, B., Wiggins, E. B., Winstead, E. L., and Rollins,

A. W.: Emission factors and evolution of SO_2 measured from biomass burning in wildfires and agricultural fires, Atmos. Chem. Phys., 22, 15603–15620, https://doi.org/10.5194/acp-22-15603-2022, 2022.

Rinne, H., Guenther, A., Greenberg, J., and Harley, P.: Isoprene and monoterpene fluxes measured above Amazonian rainforest and their dependence on light and temperature, Atmos. Environ., 36, 2421–2426, https://doi.org/10.1016/S1352-2310(01)00523-4, 2002.

Riva, M., Chen, Y., Zhang, Y., Lei, Z., Olson, N. E., Boyer, H. C., Narayan, S., Yee, L. D., Green, H. S., Cui, T., Zhang, Z., Baumann, K., Fort, M., Edgerton, E., Budisulistiorini, S. H., Rose, C. A., Ribeiro, I. O., e Oliveira, R. L., dos Santos, E. O., Machado, C. M. D., Szopa, S., Zhao, Y., Alves, E. G., de Sá, S. S., Hu, W., Knipping, E. M., Shaw, S. L., Junior, S. D., de Souza, R. A. F., Palm, B. B., Jimenez, J.-L., Glasius, M., Goldstein, A. H., Pye, H. O. T., Gold, A., Turpin, B. J., Vizuete, W., Martin, S. T., Thornton, J. A., Dutcher, C. S., Ault, A. P., and Surratt, J. D.: Increasing Isoprene Epoxydiol-to-Inorganic Sulfate Aerosol Ratio Results in Extensive Conversion of Inorganic Sulfate to Organosulfur Forms: Implications for Aerosol Physicochemical Properties, Environ. Sci. Technol., 53, 8682–8694, https://doi.org/10.1021/acs.est.9b01019, 2019.

Rollins, A. W., Kiendler-Scharr, A., Fry, J. L., Brauers, T., Brown, S. S., Dorn, H.-P., Dubé, W. P., Fuchs, H., Mensah, A., Mentel, T. F., Rohrer, F., Tillmann, R., Wegener, R., Wooldridge, P. J., and Cohen, R. C.: Isoprene oxidation by nitrate radical: alkyl nitrate and secondary organic aerosol yields, Atmos. Chem. Phys., 9, 6685–6703, https://doi.org/10.5194/acp-9-6685-2009, 2009.

Rolph, G., Stein, A., and Stunder, B.: Real-time Environmental Applications and Display sYstem: READY, Environ. Modell. Softw., 95, 210–228, https://doi.org/10.1016/j.envsoft.2017.06.025, 2017.

Saleska, S.: AmeriFlux BASE BR-Sa1 Santarem-Km67-Primary Forest, Ver. 5-5, AmeriFlux AMP [data set], https://doi.org/10.17190/AMF/1245994, 2019.

Saleska, S. R., Miller, S. D., Matross, D. M., Goulden, M. L., Wofsy, S. C., Rocha, H. R. D., Camargo, P. B. D., Crill, P., Daube, B. C., Freitas, H. C. D., Hutyra, L., Keller, M., Kirchhoff, V., Menton, M., Munger, J. W., Pyle, E. H., Rice, A. H., and Silva, H.: Carbon in Amazon Forests: Unexpected Seasonal Fluxes and Disturbance-Induced Losses, Science, 302, 1554–1557, https://doi.org/10.1126/science.1091165, 2003.

Samaké, A., Jaffrezo, J.-L., Favez, O., Weber, S., Jacob, V., Canete, T., Albinet, A., Charron, A., Riffault, V., Perdrix, E., Waked, A., Golly, B., Salameh, D., Chevrier, F., Oliveira, D. M., Besombes, J.-L., Martins, J. M. F., Bonnaire, N., Conil, S., Guillaud, G., Mesbah, B., Rocq, B., Robic, P.-Y., Hulin, A., Le Meur, S., Descheemaecker, M., Chretien, E., Marchand, N., and Uzu, G.: Arabitol, mannitol, and glucose as tracers of primary biogenic organic aerosol: the influence of environmental factors on ambient air concentrations and spatial distribution over France, Atmos. Chem. Phys., 19, 11013–11030, https://doi.org/10.5194/acp-19-11013-2019, 2019.

Sarkar, C., Guenther, A. B., Park, J.-H., Seco, R., Alves, E., Batalha, S., Santana, R., Kim, S., Smith, J., Tóta, J., and Vega, O.: PTR-TOF-MS eddy covariance measurements of isoprene and monoterpene fluxes from an eastern Amazonian rainforest, Atmos. Chem. Phys., 20, 7179–7191, https://doi.org/10.5194/acp-20-7179-2020, 2020.

Seinfeld, J. H. and Pandis, S. N.: Atmospheric chemistry and physics: from air pollution to climate change, Wiley, 2nd Edn., ISBN 9780471720188, 2006.

Shalamzari, M. S., Ryabtsova, O., Kahnt, A., Vermeylen, R., Hérent, M., Quetin-Leclercq, J., der Veken, P. V., Maenhaut, W., and Claeys, M.: Mass spectrometric characterization of organosulfates related to secondary organic aerosol from isoprene, Rapid Commun. Mass Sp., 27, 784–794, https://doi.org/10.1002/rcm.6511, 2013.

Shrivastava, M., Andreae, M. O., Artaxo, P., Barbosa, H. M. J., Berg, L. K., Brito, J., Ching, J., Easter, R. C., Fan, J., Fast, J. D., Feng, Z., Fuentes, J. D., Glasius, M., Goldstein, A. H., Alves, E. G., Gomes, H., Gu, D., Guenther, A., Jathar, S. H., Kim, S., Liu, Y., Lou, S., Martin, S. T., McNeill, V. F., Medeiros, A., de Sá, S. S., Shilling, J. E., Springston, S. R., Souza, R. A. F., Thornton, J. A., Isaacman-VanWertz, G., Yee, L. D., Ynoue, R., Zaveri, R. A., Zelenyuk, A., and Zhao, C.: Urban pollution greatly enhances formation of natural aerosols over the Amazon rainforest, Nat. Commun., 10, 1046, https://doi.org/10.1038/s41467-019-08909-4, 2019.

Sipilä, M., Berndt, T., Petäjä, T., Brus, D., Vanhanen, J., Stratmann, F., Patokoski, J., Mauldin, R. L., Hyvärinen, A.-P., Lihavainen, H., and Kulmala, M.: The Role of Sulfuric Acid in Atmospheric Nucleation, Science, 327, 1243–1246, https://doi.org/10.1126/science.1180315, 2010.

Smith, J. N. and Thomas, A. E.: Supporting data for: Seasonal Investigation of Ultrafine Particle Composition in an Eastern Amazonian Rainforest, Dryad [data set], https://doi.org/10.5061/dryad.k6djh9wgb, 2024.

Stein, A., Draxler, R., Rolph, G., Stunder, B., Cohen, M., and Ngan, F.: NOAA's HYSPLIT Atmospheric Transport and Dispersion Modeling System, B. Am. Meteorol. Soc., 96, 2059–2077, https://doi.org/10.1175/BAMS-D-14-00110.1, 2015.

Surratt, J. D., Kroll, J. H., Kleindienst, T. E., Edney, E. O., Claeys, M., Sorooshian, A., Ng, N. L., Offenberg, J. H., Lewandowski, M., Jaoui, M., Flagan, R. C., and Seinfeld, J. H.: Evidence for Organosulfates in Secondary Organic Aerosol, Environ. Sci. Technol., 41, 517–527, https://doi.org/10.1021/es062081q, 2007a.

Surratt, J. D., Lewandowski, M., Offenberg, J. H., Jaoui, M., Kleindienst, T. E., Edney, E. O., and Seinfeld, J. H.: Effect of Acidity on Secondary Organic Aerosol Formation from Isoprene, Environ. Sci. Technol., 41, 5363–5369, https://doi.org/10.1021/es0704176, 2007b.

Surratt, J. D., Gómez-González, Y., Chan, A. W. H., Vermeylen, R., Shahgholi, M., Kleindienst, T. E., Edney, E. O., Offenberg, J. H., Lewandowski, M., Jaoui, M., Maenhaut, W., Claeys, M., Flagan, R. C., and Seinfeld, J. H.: Organosulfate Formation in Biogenic Secondary Organic Aerosol, The J. Phys. Chem. A, 112, 8345–8378, https://doi.org/10.1021/jp802310p, 2008.

Szmigielski, R., Surratt, J. D., Gómez-González, Y., der Veken, P. V., Kourtchev, I., Vermeylen, R., Blockhuys, F., Jaoui, M., Kleindienst, T. E., Lewandowski, M., Offenberg, J. H., Edney, E. O., Seinfeld, J. H., Maenhaut, W., and Claeys, M.: 3-methyl-1,2,3-butanetricarboxylic acid: An atmospheric tracer for terpene secondary organic aerosol, Geophys. Res. Lett., 34, L24811, https://doi.org/10.1029/2007GL031338, 2007.

Thoma, M., Bachmeier, F., Gottwald, F. L., Simon, M., and Vogel, A. L.: Mass spectrometry-based *Aerosolomics*: a new approach to resolve sources, composition, and partitioning of secondary organic aerosol, Atmos. Meas. Tech., 15, 7137–7154, https://doi.org/10.5194/amt-15-7137-2022, 2022.

Varanda Rizzo, L., Roldin, P., Brito, J., Backman, J., Swietlicki, E., Krejci, R., Tunved, P., Petäjä, T., Kulmala, M., and Artaxo, P.: Multi-year statistical and modeling analysis of submicrometer aerosol number size distributions at a rain forest site in Amazonia, Atmos. Chem. Phys., 18, 10255–10274, https://doi.org/10.5194/acp-18-10255-2018, 2018.

Varble, A. C., Igel, A. L., Morrison, H., Grabowski, W. W., and Lebo, Z. J.: Opinion: A critical evaluation of the evidence for aerosol invigoration of deep convection, Atmos. Chem. Phys., 23, 13791–13808, https://doi.org/10.5194/acp-23-13791-2023, 2023.

von Glasow, R. and Crutzen, P. J.: Model study of multiphase DMS oxidation with a focus on halogens, Atmos. Chem. Phys., 4, 589–608, https://doi.org/10.5194/acp-4-589-2004, 2004.

Wang, J., Krejci, R., Giangrande, S., Kuang, C., Barbosa, H. M. J., Brito, J., Carbone, S., Chi, X., Comstock, J., Ditas, F., Lavric, J., Manninen, H. E., Mei, F., Moran-Zuloaga, D., Pöhlker, C., Pöhlker, M. L., Saturno, J., Schmid, B., Souza, R. A. F., Springston, S. R., Tomlinson, J. M., Toto, T., Walter, D., Wimmer, D., Smith, J. N., Kulmala, M., Machado, L. A. T., Artaxo, P., Andreae, M. O., Petäjä, T., and Martin, S. T.: Amazon boundary layer aerosol concentration sustained by vertical transport during rainfall, Nature, 539, 416–419, https://doi.org/10.1038/nature19819, 2016.

Wang, M. and Penner, J. E.: Aerosol indirect forcing in a global model with particle nucleation, Atmos. Chem. Phys., 9, 239–260, https://doi.org/10.5194/acp-9-239-2009, 2009.

Weigel, R., Borrmann, S., Kazil, J., Minikin, A., Stohl, A., Wilson, J. C., Reeves, J. M., Kunkel, D., de Reus, M., Frey, W., Lovejoy, E. R., Volk, C. M., Viciani, S., D'Amato, F., Schiller, C., Peter, T., Schlager, H., Cairo, F., Law, K. S., Shur, G. N., Belyaev, G. V., and Curtius, J.: In situ observations of new particle formation in the tropical upper troposphere: the role of clouds and the nucleation mechanism, Atmos. Chem. Phys., 11, 9983–10010, https://doi.org/10.5194/acp-11-9983-2011, 2011.

Westervelt, D. M., Pierce, J. R., Riipinen, I., Trivitayanurak, W., Hamed, A., Kulmala, M., Laaksonen, A., Decesari, S., and Adams, P. J.: Formation and growth of nucleated particles into cloud condensation nuclei: model–measurement comparison, Atmos. Chem. Phys., 13, 7645–7663, https://doi.org/10.5194/acp-13-7645-2013, 2013.

Williamson, C. J., Kupc, A., Axisa, D., Bilsback, K. R., Bui, T., Campuzano-Jost, P., Dollner, M., Froyd, K. D., Hodshire, A. L., Jimenez, J. L., Kodros, J. K., Luo, G., Murphy, D. M., Nault, B. A., Ray, E. A., Weinzierl, B., Wilson, J. C., Yu, F., Yu, P., Pierce, J. R., and Brock, C. A.: A large source of cloud condensation nuclei from new particle formation in the tropics, Nature, 574, 399–403, https://doi.org/10.1038/s41586-019-1638-9, 2019.

Yáñez-Serrano, A. M., Nölscher, A. C., Bourtsoukidis, E., Gomes Alves, E., Ganzeveld, L., Bonn, B., Wolff, S., Sa, M., Yamasoe, M., Williams, J., Andreae, M. O., and Kesselmeier, J.: Monoterpene chemical speciation in a tropical rainforest:variation with season, height, and time of dayat the Amazon Tall Tower Observatory (ATTO), Atmos. Chem. Phys., 18, 3403–3418, https://doi.org/10.5194/acp-18-3403-2018, 2018.

Yáñez-Serrano, A. M., Bourtsoukidis, E., Alves, E. G., Bauwens, M., Stavrakou, T., Llusià, J., Filella, I., Guenther, A., Williams, J., Artaxo, P., Sindelarova, K., Doubalova, J., Kesselmeier, J., and Peñuelas, J.: Amazonian biogenic volatile organic compounds under global change, Global Change Biol., 26, 4722–4751, https://doi.org/10.1111/gcb.15185, 2020.

Yee, L. D., Isaacman-VanWertz, G., Wernis, R. A., Meng, M., Rivera, V., Kreisberg, N. M., Hering, S. V., Bering, M. S., Glasius, M., Upshur, M. A., Gray Bé, A., Thomson, R. J., Geiger, F. M., Offenberg, J. H., Lewandowski, M., Kourtchev, I., Kalberer, M., de Sá, S., Martin, S. T., Alexander, M. L., Palm, B. B., Hu, W., Campuzano-Jost, P., Day, D. A., Jimenez, J. L., Liu, Y., McKinney, K. A., Artaxo, P., Viegas, J., Manzi, A., Oliveira, M. B., de Souza, R., Machado, L. A. T., Longo, K., and Goldstein, A. H.: Observations of sesquiterpenes and their oxidation products in central Amazonia during the wet and dry seasons, Atmos. Chem. Phys., 18, 10433–10457, https://doi.org/10.5194/acp-18-10433-2018, 2018.

Zhang, Y., Chen, Y., Lambe, A. T., Olson, N. E., Lei, Z., Craig, R. L., Zhang, Z., Gold, A., Onasch, T. B., Jayne, J. T., Worsnop, D. R., Gaston, C. J., Thornton, J. A., Vizuete, W., Ault, A. P., and Surratt, J. D.: Effect of the Aerosol-Phase State on Secondary Organic Aerosol Formation from the Reactive Uptake of Isoprene-Derived Epoxydiols (IEPOX), Environ. Sci. Technol. Lett., 5, 167–174, https://doi.org/10.1021/acs.estlett.8b00044, 2018.

Zhao, B., Shrivastava, M., Donahue, N. M., Gordon, H., Schervish, M., Shilling, J. E., Zaveri, R. A., Wang, J., Andreae, M. O., Zhao, C., Gaudet, B., Liu, Y., Fan, J., and Fast, J. D.: High concentration of ultrafine particles in the Amazon free troposphere produced by organic new particle formation, P. Natl. Acad. Sci. US, 117, 25344–25351, https://doi.org/10.1073/pnas.2006716117, 2020.